

Spectroscopic performance of High-Z Sensor Materials

Paul Sellin

Department of Physics

University of Surrey, Guildford, GU2 7XH, UK

p.sellin@surrey.ac.uk

Contents

Overview of High-Z detector materials

Charge transport and spectroscopy

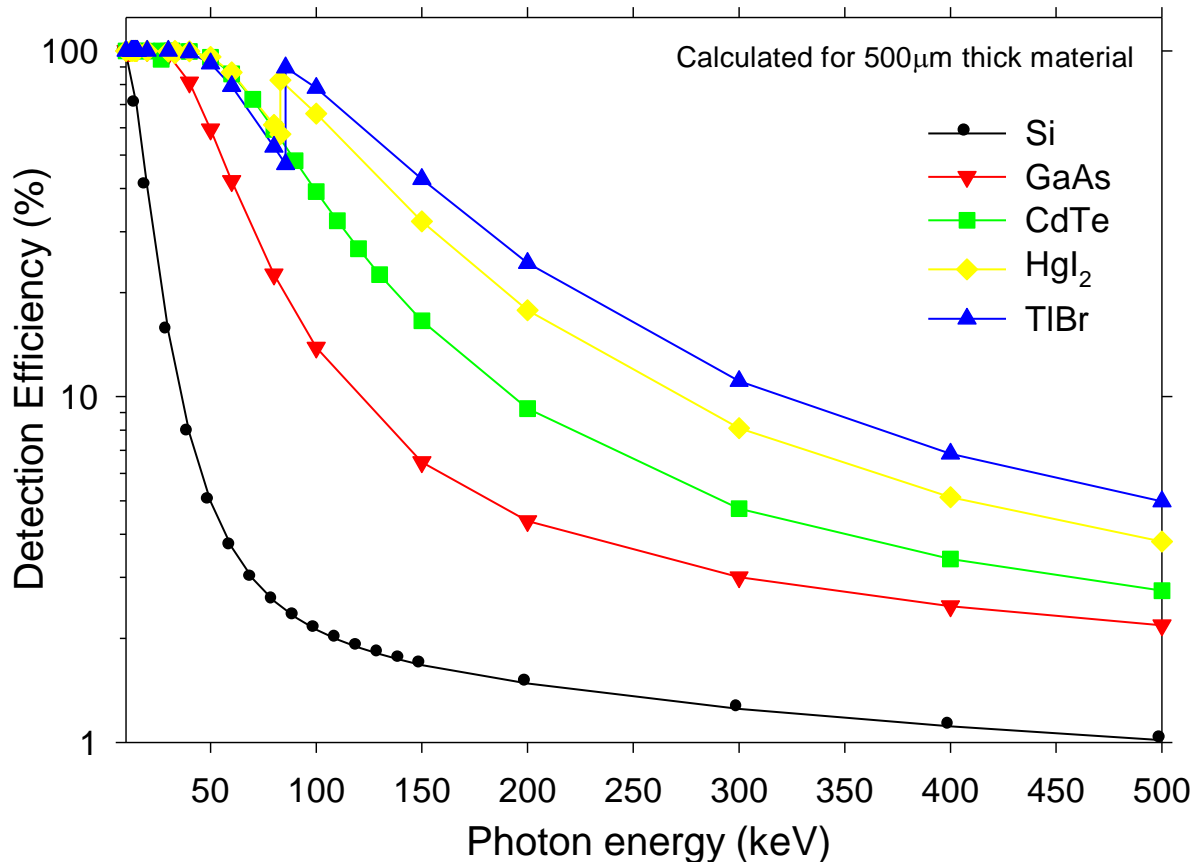
Signal formation in pixel detectors

Current status of key materials:

- CZT and CdTe
- GaAs
- TlBr
- Other materials

High-Z materials for gamma and X-ray detection

For gammas and X-rays, the detection efficiency is highly dependent on the atomic number 'Z' of the detecting material



Compound semiconductors (e.g. GaAs or CdTe) have been increasingly developed for use as X-ray detectors

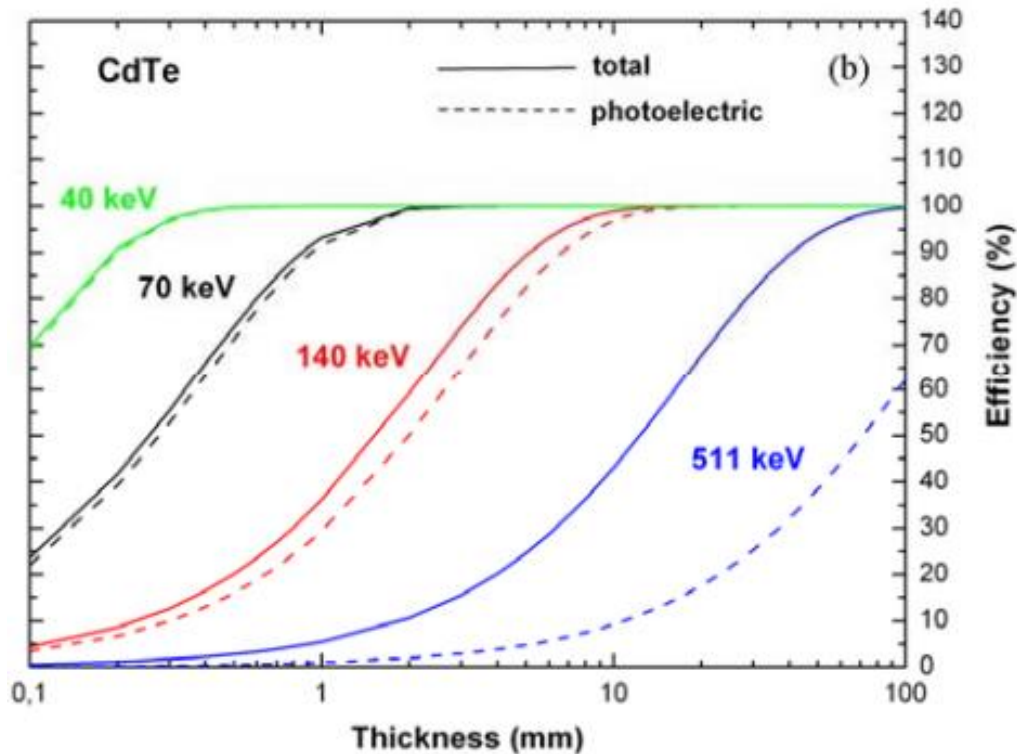
These compounds provide moderately high-Z detector materials, eg. **CdTe** with $Z_{Cd} = 48$ and $Z_{Te} = 52$,

The ternary alloy **CdZnTe (CZT)** has almost identical detection efficiency

As we have heard this morning, **germanium** is also a high-Z semiconductor which has unique requirements for cryogenic cooling.

Detection efficiency in thin detectors

For pixel detector applications at lower energies thin detectors provide sufficient detection efficiency. For example, CdTe is normally obtained with 0.5mm or 1mm thickness and has good efficiency for energies up to 50 keV:



The mean free path lengths of the Cd and Te K_{α} and K_{β} fluorescence are long:

- 119 μm and 62 μm respectively
- High yields: 84.3% and 87.7%

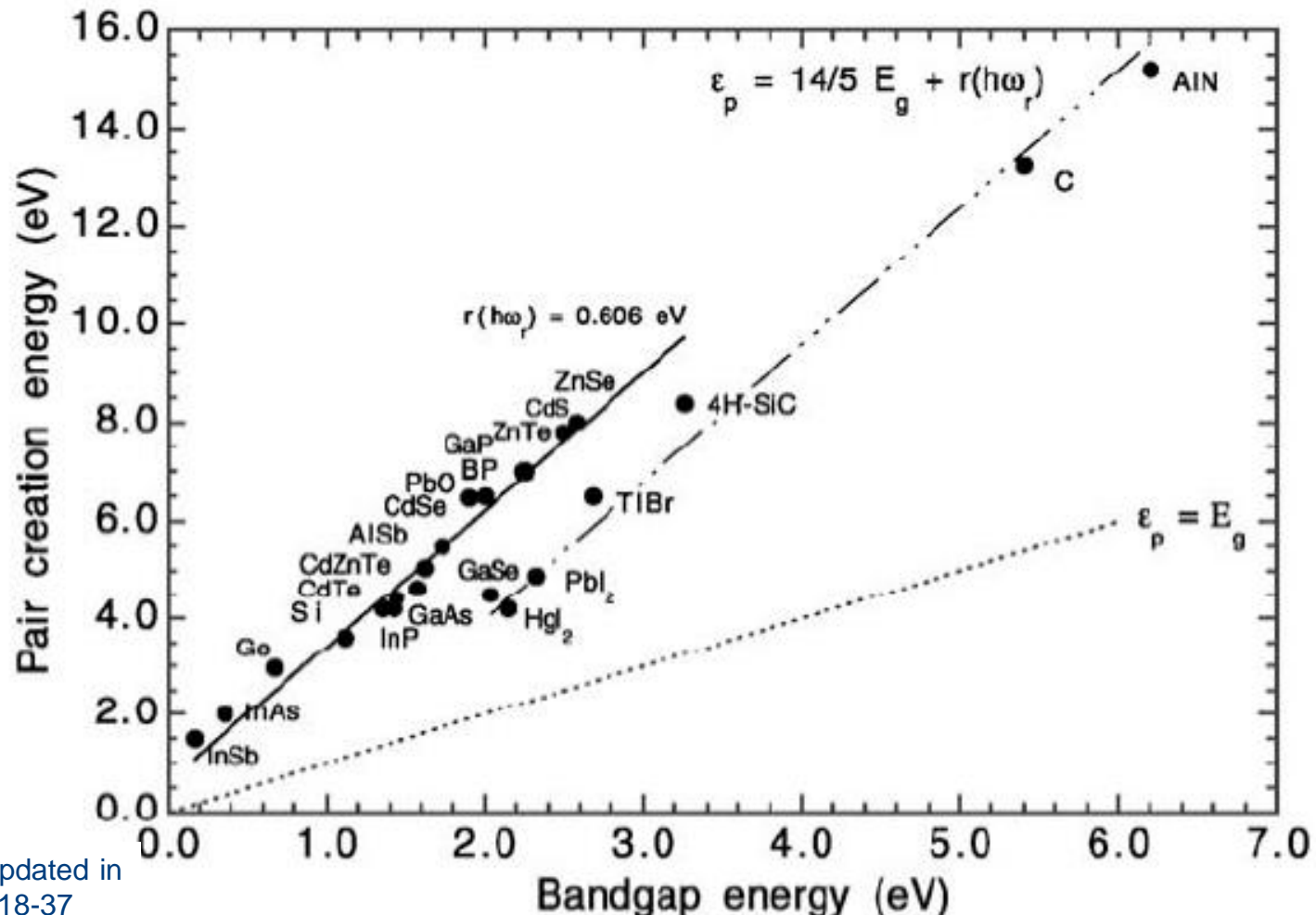
This reduces the spatial and spectroscopic resolution of small pixel detectors with CdTe sensors

New sensor materials

The Klein chart shows the relationship between **electron-hole pair creation energy** (often called the 'W value') and **bandgap**:

There are many interesting candidate sensor materials, beyond CdTe/CZT and GaAs, eg:

- TlBr
- CdMnTe
- GaN
- Diamond



Resolution limits in real detectors

To optimise detector performance we should understand the various factors that limit spectroscopic resolution in real detectors:

Detection Efficiency

Photoelectric quantum efficiency is strongly dependent on Z. Compton Scatter reduces photopeak efficiency

Fano Factor

Charge generation statistics limit detector resolution, defined by the Electron-Hole Pair creation energy and Fano factor

Sensor polarisation


Time dependent changes in bulk electric field cause spectral degradation

Fluorescence X-rays

Characteristic X-rays emitted from the detector material can cause escape events

Charge Trapping

Incomplete charge transport reduces the signal amplitude and degrades resolution



	Z	K-edge [keV]	L1-edge [keV]	L2-edge [keV]	L3-edge [keV]	α_1 [keV]	$k\alpha_2$ [keV]	$d_{\alpha 1}$ [μm]	$d_{\alpha 2}$ [μm]	ω_K
Si	14	1.839	0.150	0.100	0.100	1.74	1.739	11.86	11.86	0.041
Ga	31	10.367	1.298	1.142	1.115	9.25	9.225	40.62	40.28	0.505
Ge	32	11.110	1.426	1.259	1.228	9.89	9.856	50.85	50.40	0.548
As	33	11.867	1.527	1.359	1.323	10.54	10.508	15.62	15.47	0.566
Cd	48	26.711	4.018	3.727	3.538	23.17	22.984	113.2	110.7	0.836
Te	52	31.814	4.939	4.612	4.341	27.44	27.202	59.32	57.85	0.873

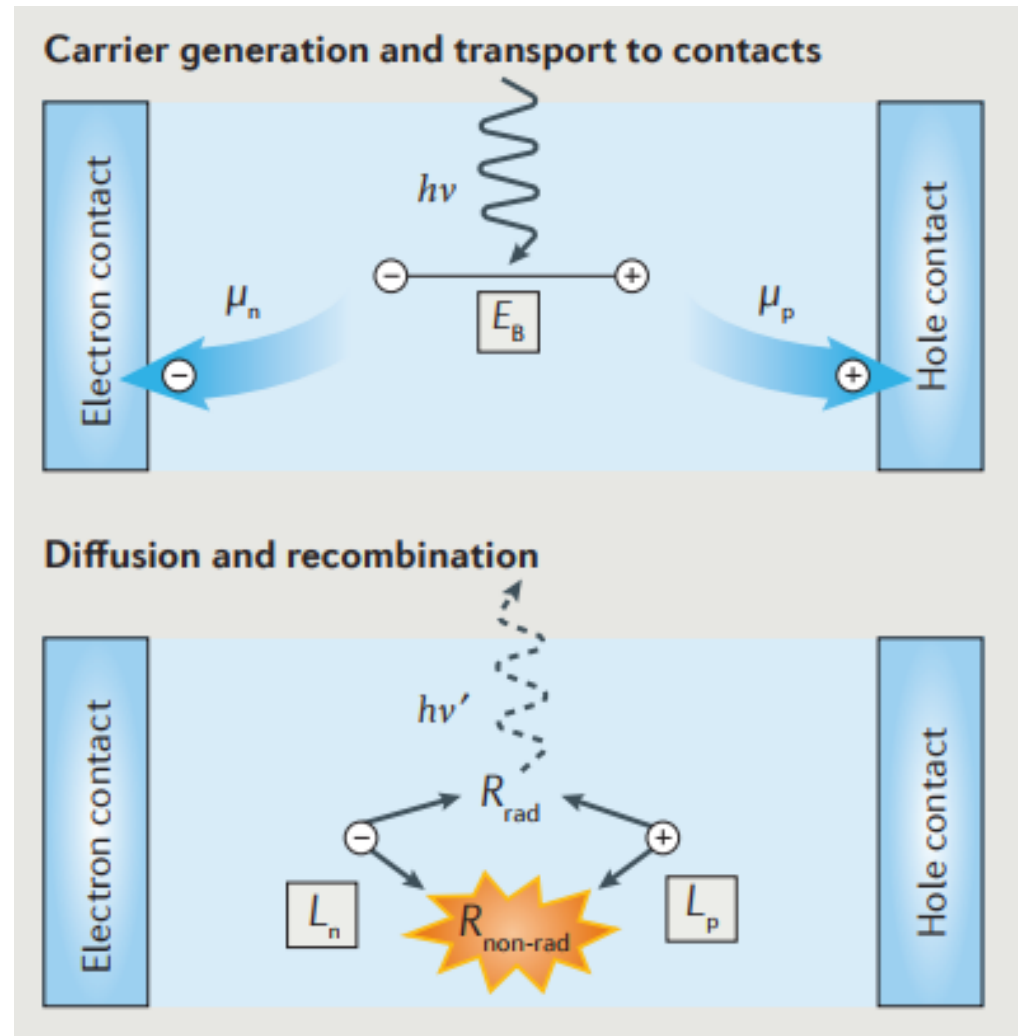
Charge Transport in semiconductors

A radiation interaction creates carriers which are either free and/or excitonically bound, determined by the exciton binding energy (E_B), sample temperature and carrier density.

Free carriers can either diffuse or drift, depending on the presence of an electric field, with associated mobilities μ_n , and μ_p

Carriers have an average recombination lifetime τ before they recombine, during which they drift or diffuse.

The lifetime is determined by the recombination rate, a result of radiative and non-radiative processes



Time of Flight (TOF)

To directly measure drift mobility μ the Time of Flight (TOF) method is used:

- ❑ the **drift time** of the electrons and/or holes are directly measured from the pulse shape induced in the external circuit
- ❑ either **current pulses** or **charge pulses** can be used

Drift velocity is related to μ , such that: $v_{dr} = \mu E = \frac{d}{t_{dr}}$

Electrons and holes are generated using a fast laser pulse (or alpha particles).

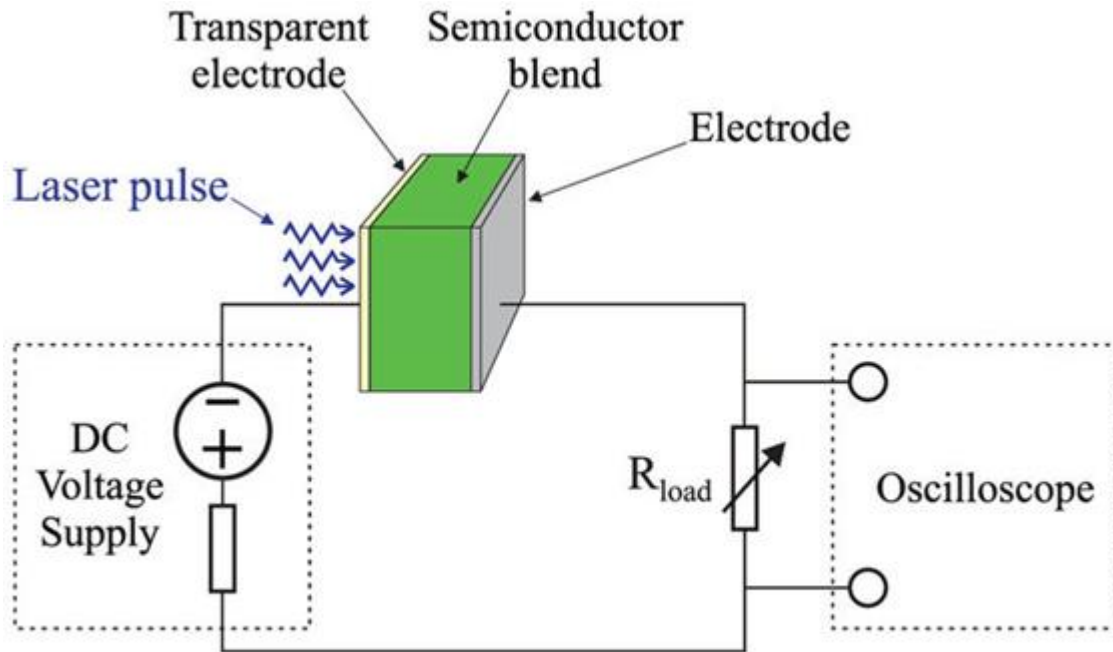
TOF relies on two assumptions:

- ❑ The measured carrier drift time is not limited by trapping, ie. at least some of the **carriers reach the electrodes**, so the drift distance is known.
- ❑ The field strength is uniform through the device.

For single carrier transport, the mobility is given by:

$$\mu = \frac{d^2}{\tau_{dr} V}$$

Time of Flight technique



In its general form, a laser pulse is used to excite charge carriers

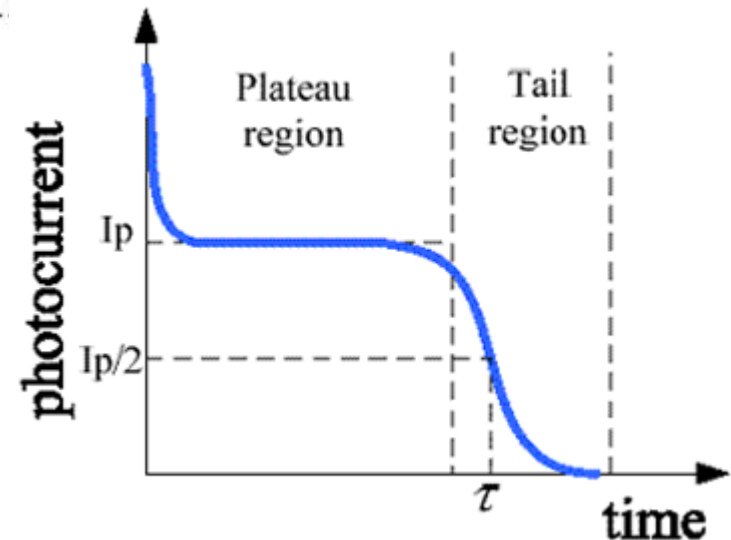
Electrons and hole drift under the influence of an applied field

A photocurrent pulse is measured in an external circuit

The form of the current pulse:

Plateau region, as the carriers drift through the semiconductor with a drift time t

Tail region, there can be a range of drift times across the semiconductor, with a mean drift time t



Room temperature mobility in CdTe

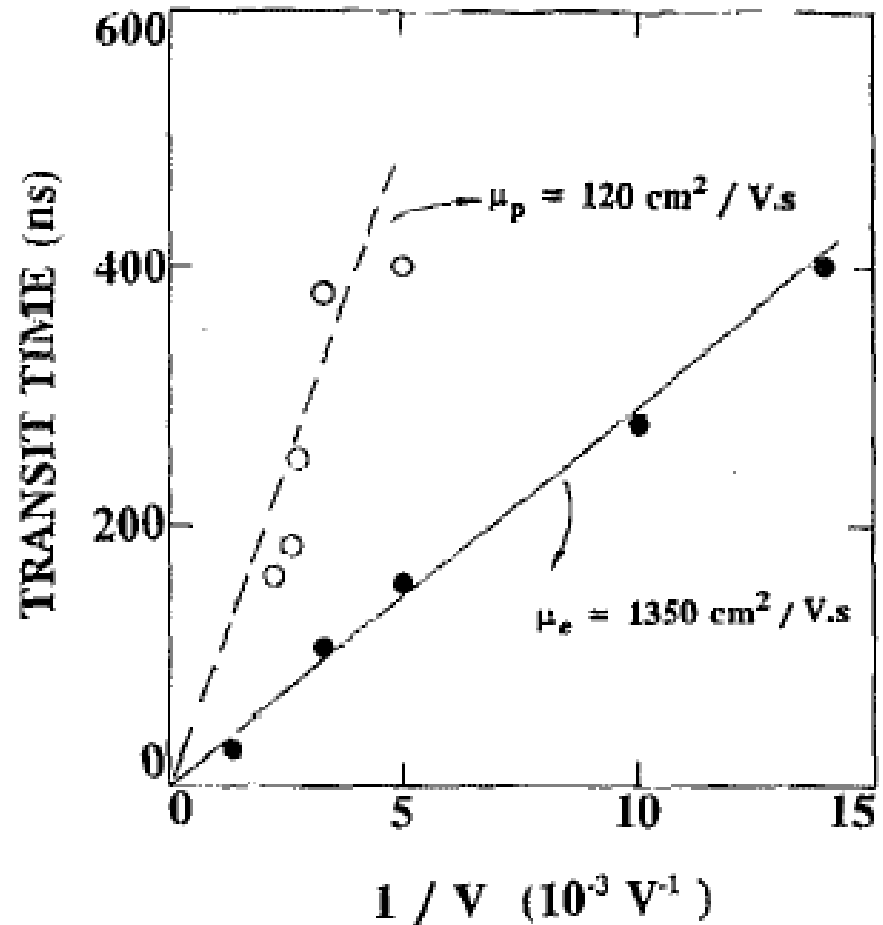
Mobility is extracted from drift time data as a function of field strength. This can be graphed in many different forms:

- velocity vs field, gradient is μ
- drift time vs $1/V$, gradient is d^2/μ

$$\mu = \frac{v}{E} = \frac{d^2}{V t_{dr}}$$

Drift mobility of electrons and holes measured in CdTe

Z. Burshtein et al, APL 63 (1993) 102-104



Mobility and Trapping

Both electron and hole mobility can be affected by the presence of traps in the material

Typical mobility and lifetime values for CdTe:

μ_e (300K)	μ_h (300K)	τ_e	τ_h
800-1100 cm ² /Vs	60-90 cm ² /Vs	~1 μ s	~1 μ s

Temperature dependent mobility $\Rightarrow \mu_e$ increases at lower temperature, μ_h decreases.

Scattering mechanisms alone cannot describe the temperature variations – need a trap-controlled mobility model:

$$\mu = \mu_0 \left(1 + \frac{N_T}{N_C} \exp\left(\frac{E_T}{kT}\right) \right)^{-1}$$

μ_0 – scattering-limited mobility

E_T, N_T – trap energy and concentration

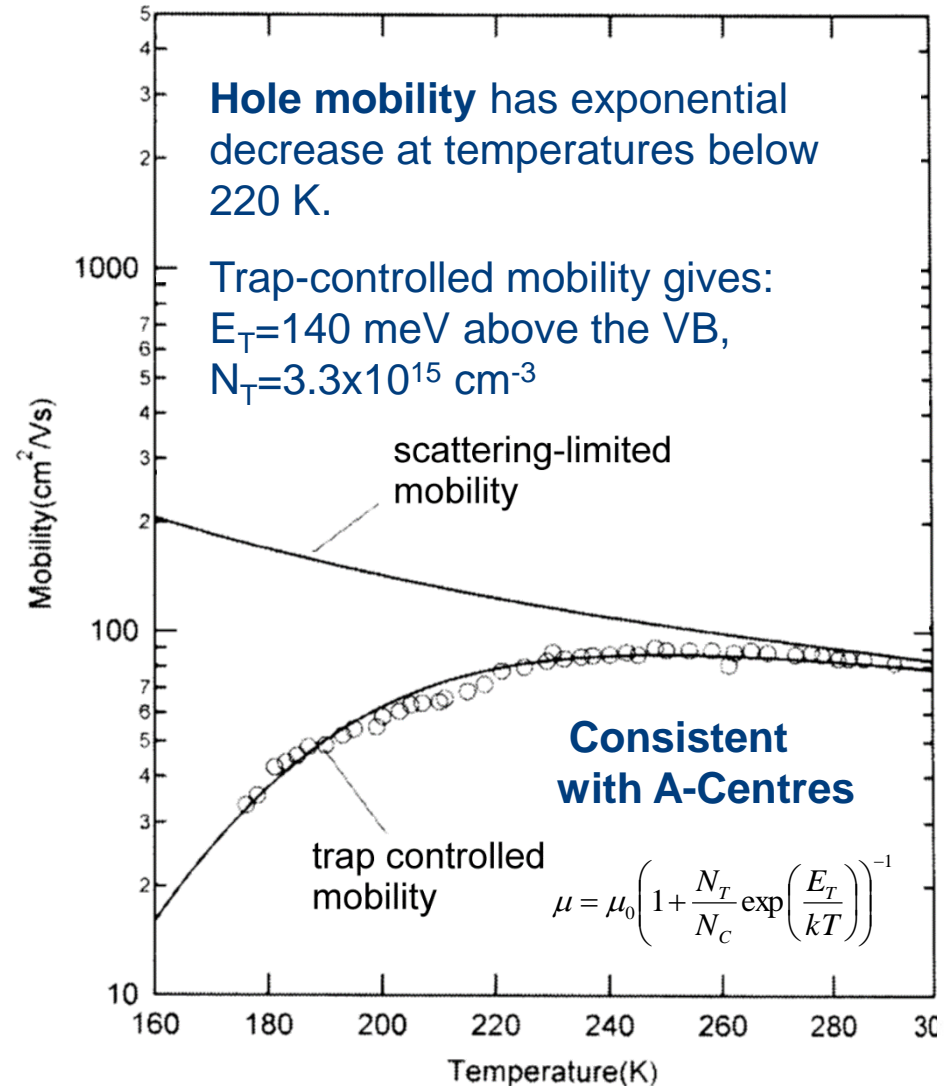
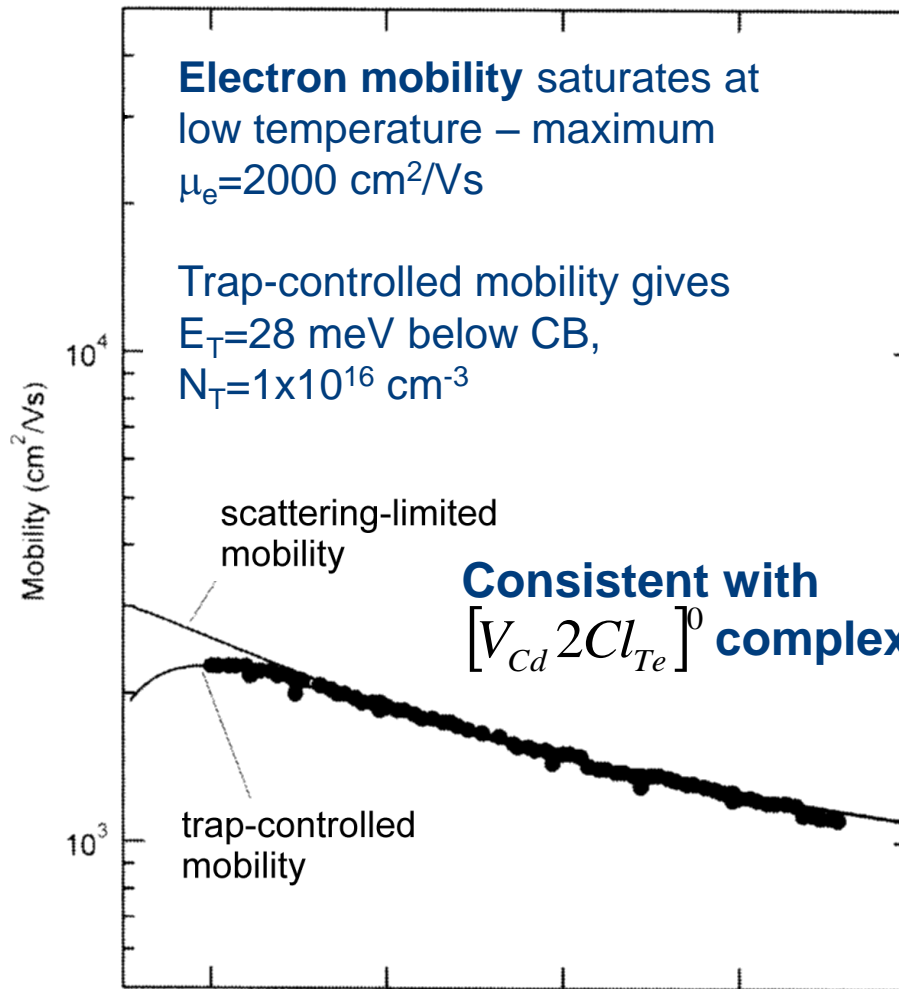
N_C – effective density of states at bend edge

In CdTe electron trapping is associated with a complex defect: $[V_{Cd} 2Cl_{Te}]^0$
2 Cl donors on Te site + Cd vacancy

Hole trapping is associated with shallow Cd-vacancies (V_{Cd}) and A-Centers (V_{Cd} -donor complex), acting as single and double acceptors.

Drift mobility in CdTe

TOF mobility measurements of CdTe vs Temperature show the dominant conduction mechanisms:



Drift mobility at high charge injection

At high charge injection carrier mobility drops due to increased scattering between electrons and holes.

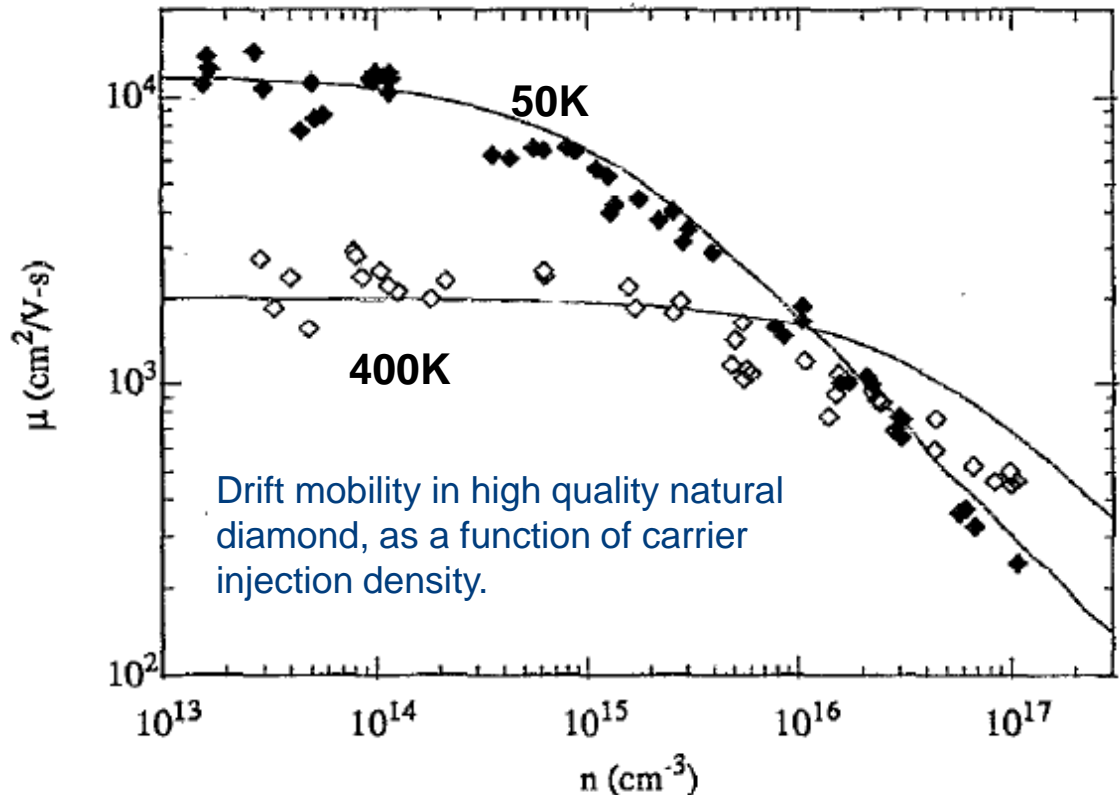
This effect has been observed in X-ray detectors used in high beam fluxes, such as at synchrotrons

The effective mobility μ is a combination of:

- the carrier-carrier limited mobility μ_{CC}
- the mobility due to conventional scattering mechanisms such as phonon and impurity scattering, μ_0 :

Using Mathiessen's rule, these contributions are combined as:

$$\frac{1}{\mu} = \frac{1}{\mu_0} + \frac{1}{\mu_{CC}}$$



The data shows a significant decrease in effective mobility in diamond for charge densities above 10^{15} cm^{-3} .

Mobility-Lifetime product

For a detector the charge drift distance λ is a fundamental measure of material quality, often measured by the mobility-lifetime product $\mu\tau$, where:

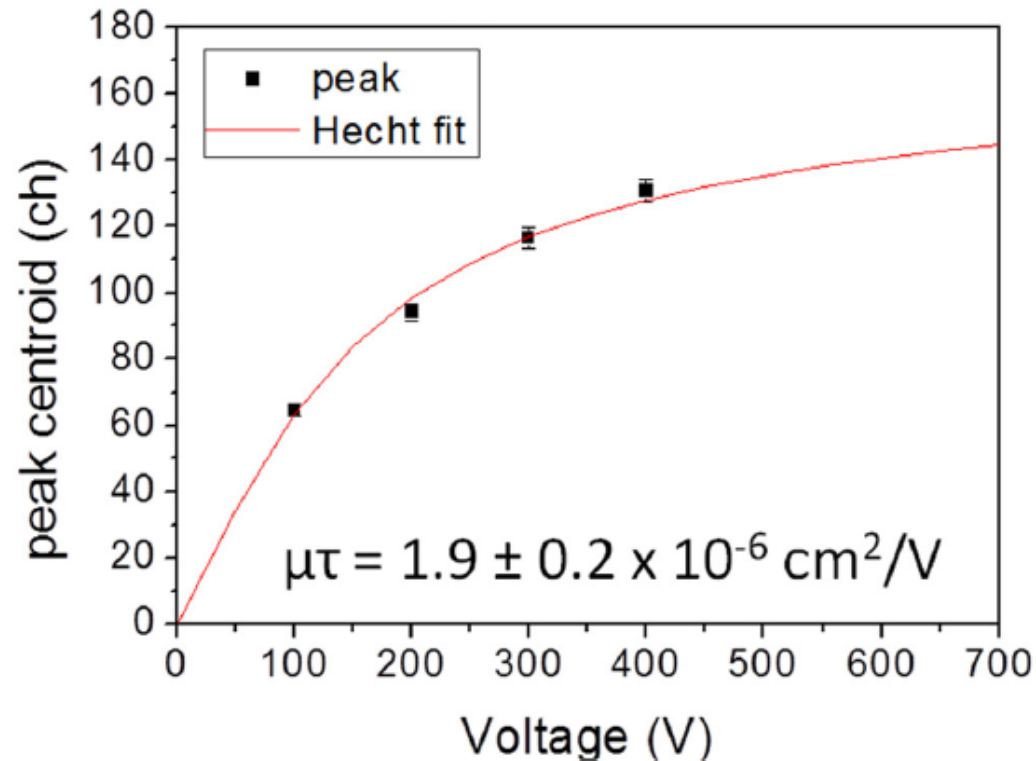
$$\lambda = \mu\tau E$$

The Hecht plot shows the increase in the mean pulse height as a function of bias voltage

For a single carrier type (either electrons or holes) we fit the Hecht plot using:

$$\eta = \frac{\mu\tau \cdot V}{d^2} \left[1 - \exp\left(-\frac{d^2}{\mu\tau \cdot V}\right) \right]$$

and hence obtain effective $\mu\tau$ value for the material.



In a pixel detector the Hecht equation is not accurate and corrections are required

Induced signals – planar detector

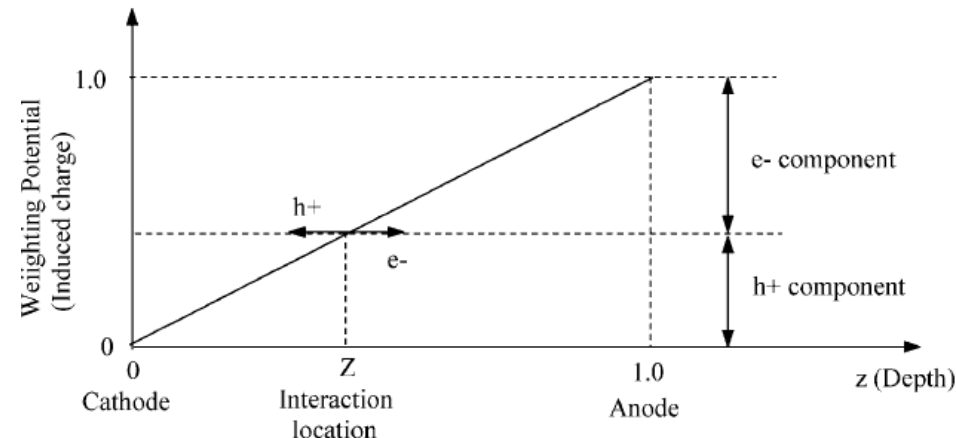
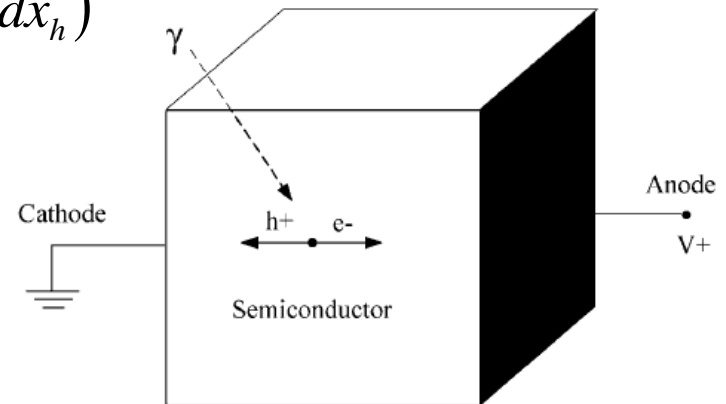
In a planar detector, where N_0 electron-hole pairs are generated per event, the induced charge dQ is expressed in terms of electron and hole drift lengths (dx_e and dx_h) respectively:

Ramo's theorem:
$$dQ = \frac{qN_0}{d} (dx_e + dx_h)$$

The separate contributions from holes and electrons are combined - both carrier types travel completely across the detector

⇒ for a point interaction at a depth half-way through a detector, the electrons and holes contribute equally to the total induced charge

In a planar detector the same induced signal is generated at either electrode (but inverted)



Pixel Detectors and Weighting Field

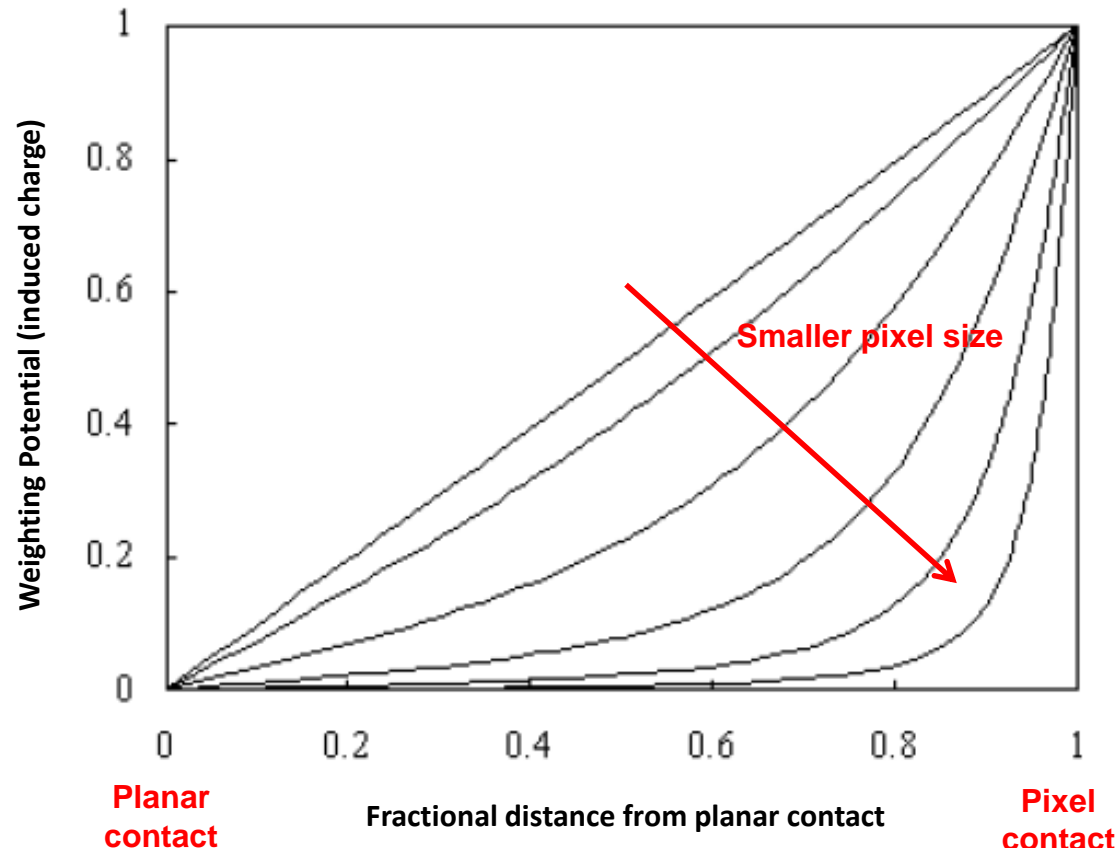
For pixel detectors the signal induced in any particular pixel is not the same as the signal induced on the planar contact

We need to consider how the drifting charges induce a current in all the electrodes. The Weighting Field \mathbf{E}_W describes the electrostatic coupling between a moving charge and the sensing electrode.

The induced current is given by:

$$i = -q \mathbf{E}_W \cdot \mathbf{v}$$

where \mathbf{v} is the drift velocity of the moving charge

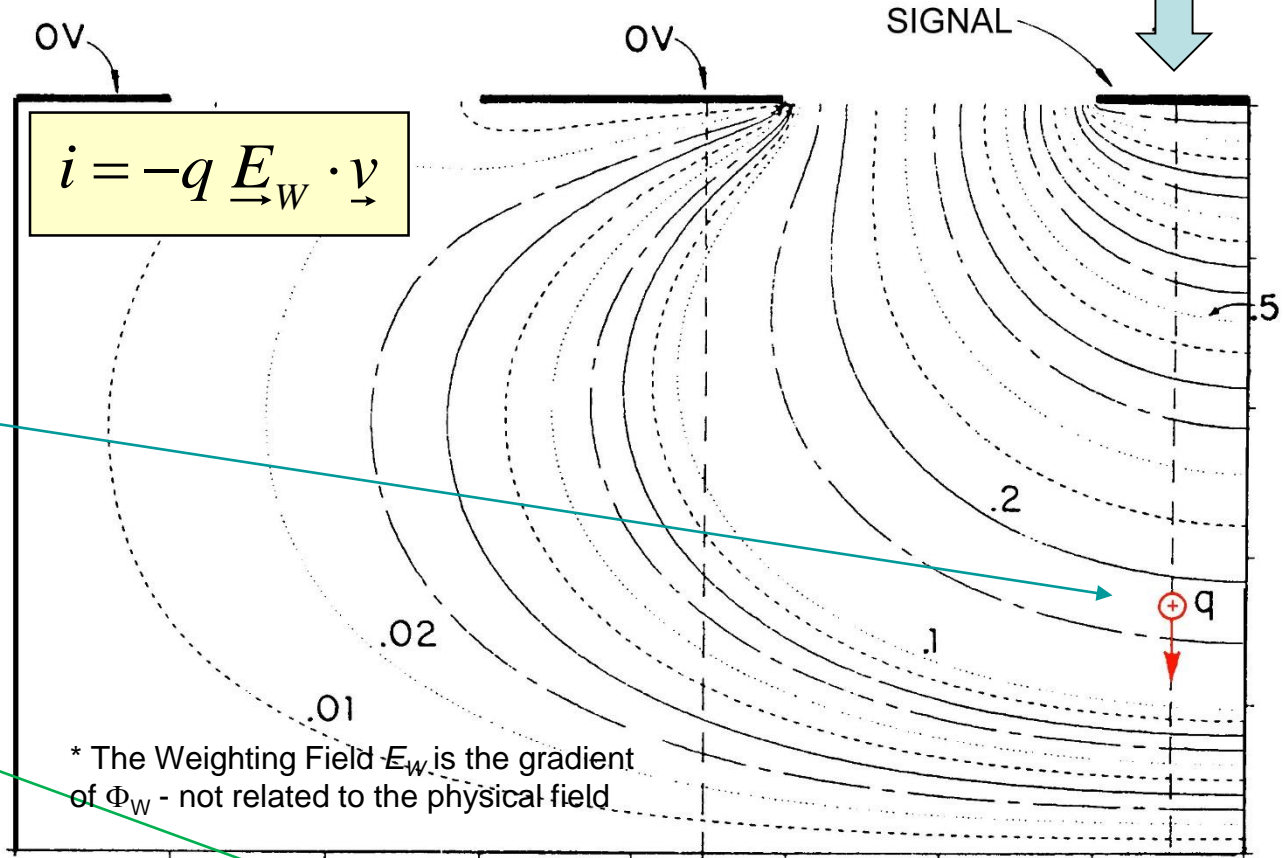


Pixel weighting fields (1)

Consider a pixel detector:
the weighting field \underline{E}_W is highly non-uniform*

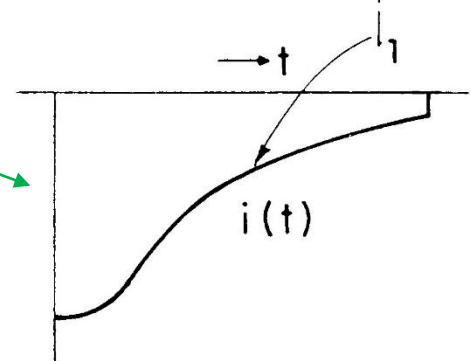
Here the charge is drifting away from the pixel:

- charge q drifts in the physical field
- the current pulse decreases, due to reducing \underline{E}_W
- assumes that the drift velocity is constant



* The Weighting Field \underline{E}_W is the gradient of Φ_W - not related to the physical field

If the charge drifts the complete distance, the total induced charge is $\int i(t) dt = q$



Pixel weighting fields (2)

In the neighbouring pixel the induced current pulse is complex:

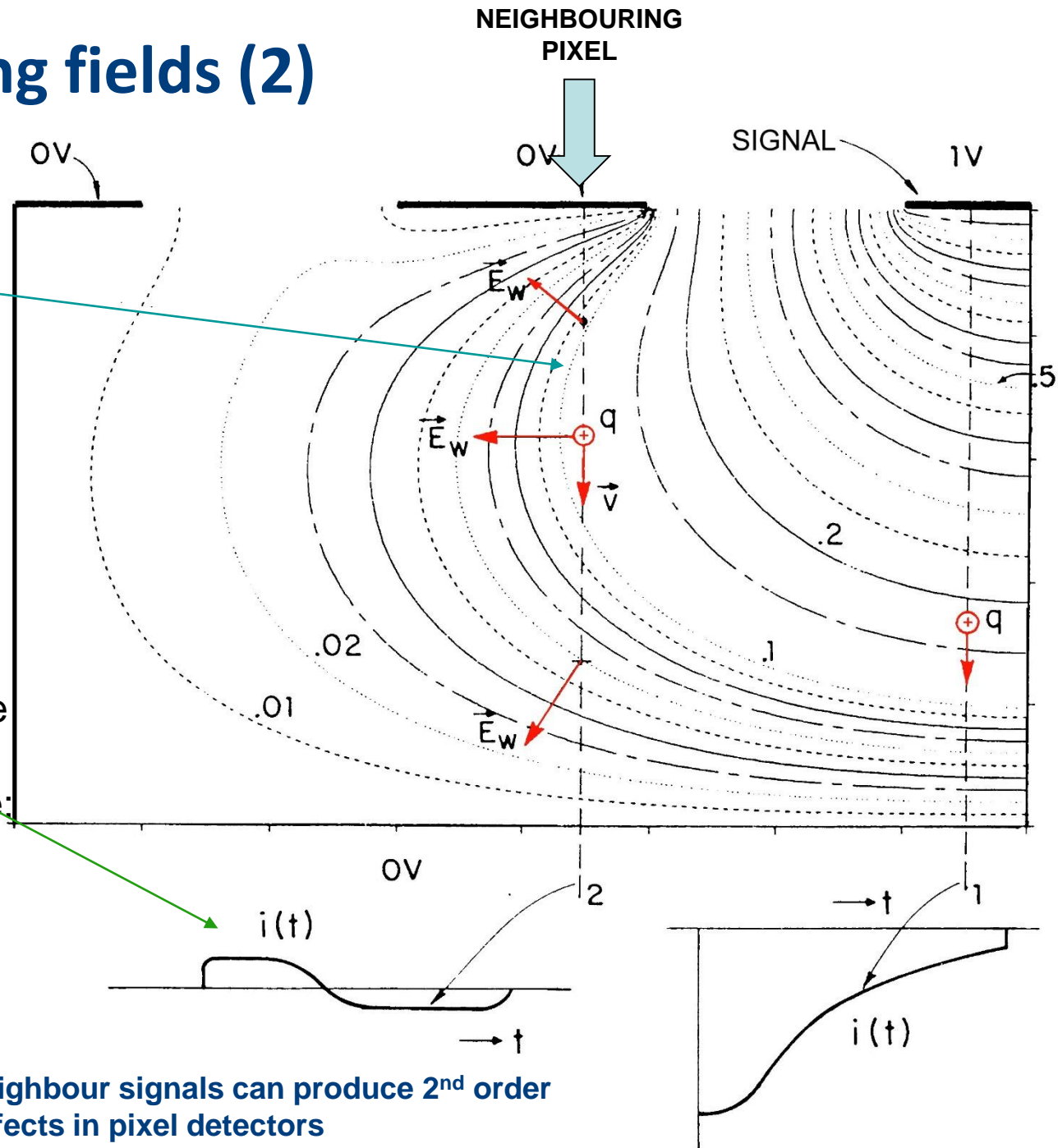
Since:

$$i = -q \vec{E}_w \cdot \vec{v}$$

- the current pulse changes sign as the charge drifts across the device
- if the charge crosses the complete device, the induced charge is zero, i.e:

$$q = \int i(t) dt = 0$$

but there is a measurable current pulse!



These induced neighbour signals can produce 2nd order effects in pixel detectors

Hecht plot for small pixels

In a small pixel detector, the weighting field introduces a significant correction to how the induced signal couples to the pixel electrode.

In this case the classical Hecht equation is not applicable, and a modified expression must be used:

$$Q(U) = Q_0 \cdot \frac{d}{\mu\tau \cdot (U - U_0)} \cdot \int_0^d w(x) \cdot e^{-\frac{-x \cdot d}{\mu\tau \cdot (U - U_0)}} dx + e^{-\frac{d^2}{\mu\tau \cdot (U - U_0)}}$$

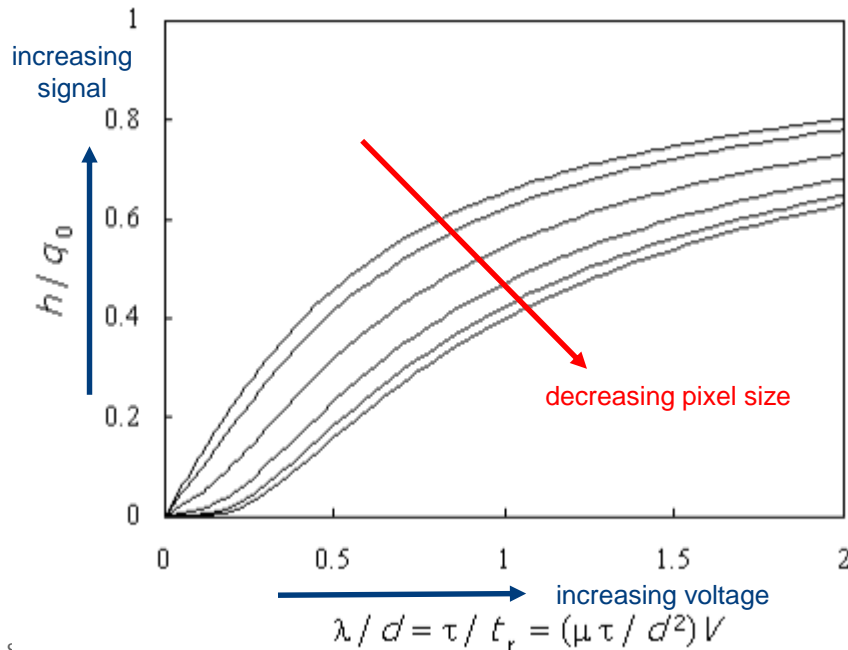
where:

Q_0 is the charge generated

d is the detector thickness

U_0 is a bias offset threshold

$w(x)$ is the pixel weighting potential as a function of distance x from the cathode



The modified Hecht expression tends towards a “S shape” at small pixel sizes

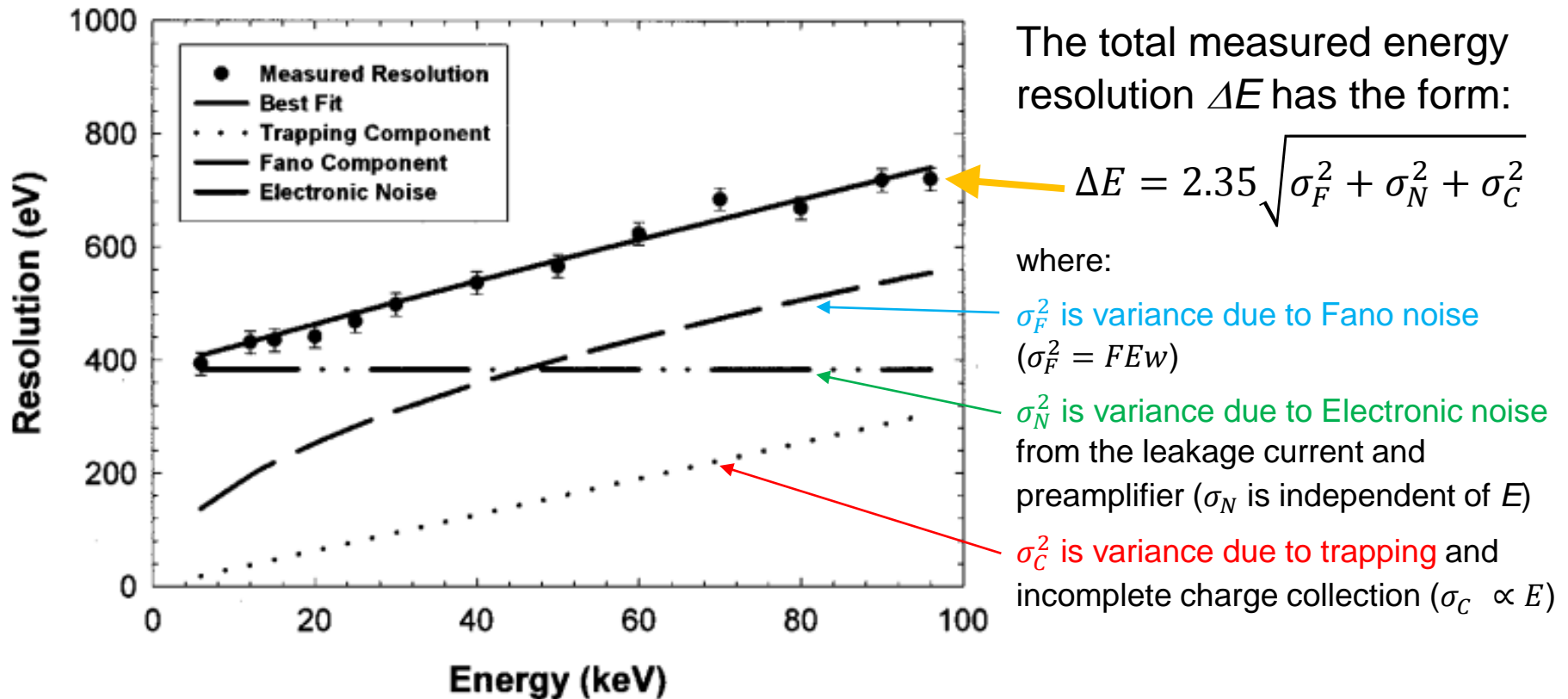
At low voltage a significant amount of charge is trapped before nearing the pixel, and the induced charge is less

P. Smolyanskiy et al, Properties of GaAs:Cr Timepix detectors, 13 (2018) T02005

U. Lachish, Electron lifetime determination in semiconductor gamma detector arrays, arXiv:1701.03459.

Fano limited energy resolution

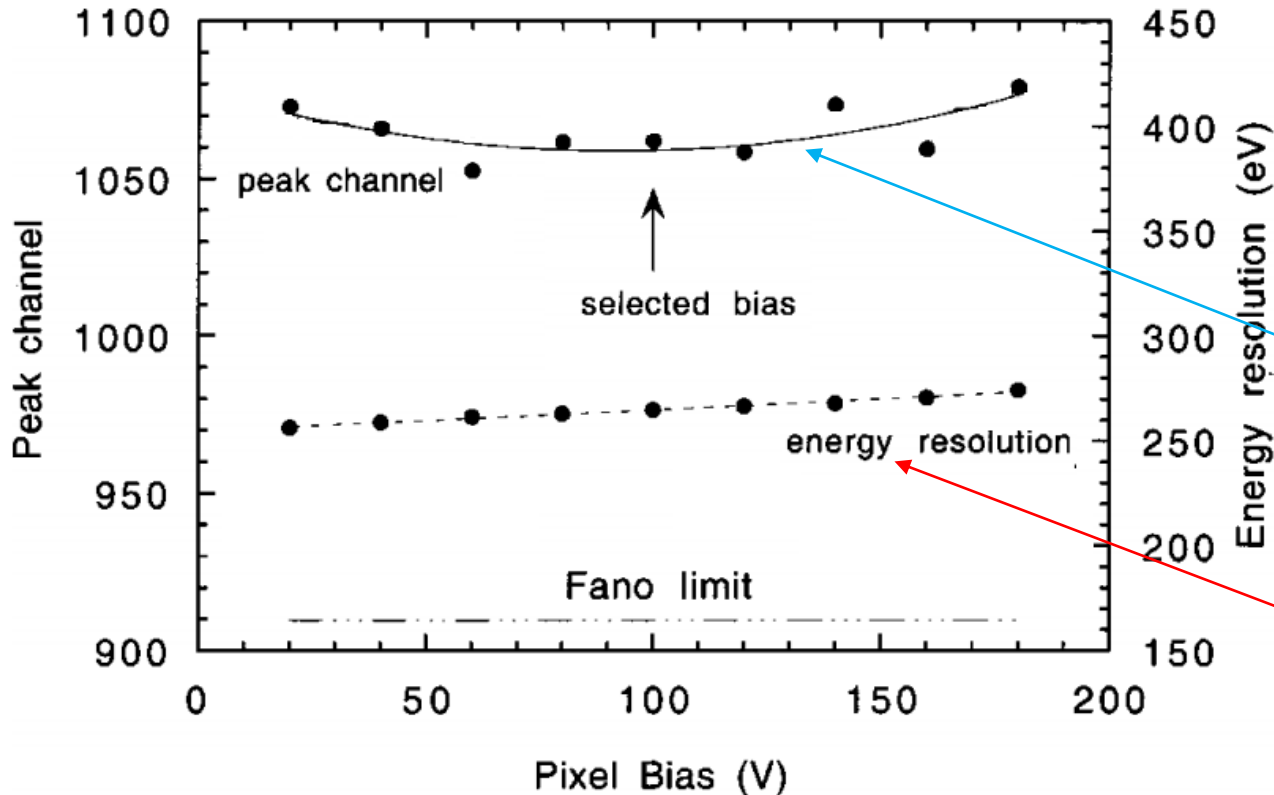
For the highest quality detector materials, the detector resolution can approach the intrinsic limit imposed by the Fano resolution.



Data taken from a GaAs detector pixel with a **resolution of 700 eV** at 98 keV

Fano limited energy resolution (2)

At high detector resolution, small affects can be observed as a function of bias voltage:



GaAs pixel detector resolution measured at -40C using ^{55}Fe

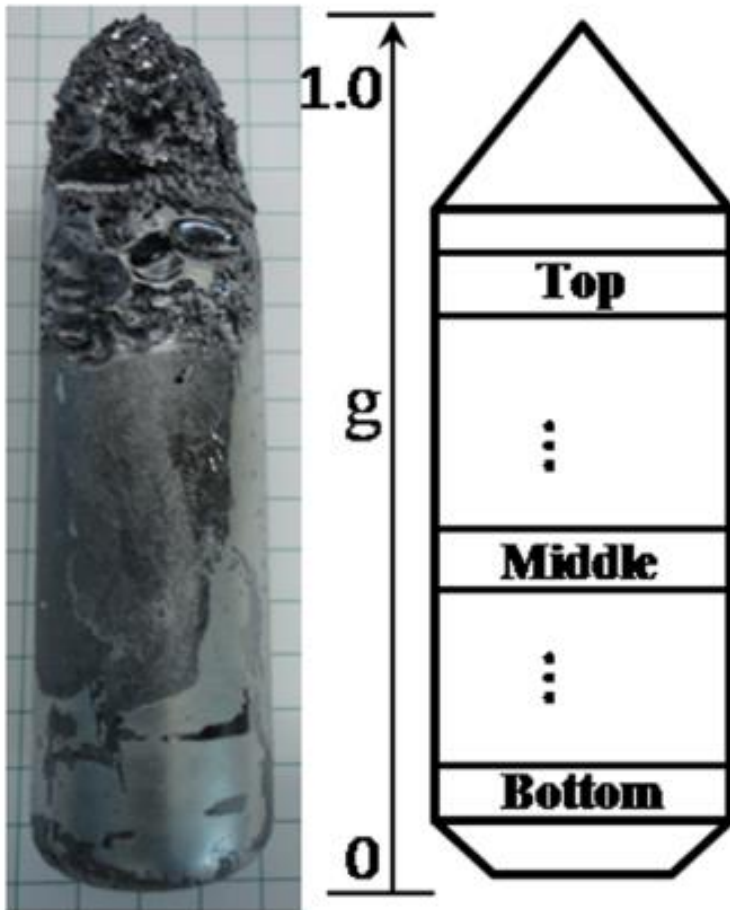
As the detector is fully depleted the peak position only varies weakly with bias voltage, due to small changes in the carrier mobility

There is a small degradation in energy resolution due to increasing leakage current.

At 100V: resolution at -40C is 375 eV FWHM. At room temperature, 660 eV FWHM

Overview of CZT and CdTe

CZT is the dominant “high Z” detector materials, and the commercial availability of high quality “single crystal” material has improved significantly



CZT crystal growth is complex! Generally crystal growers require:

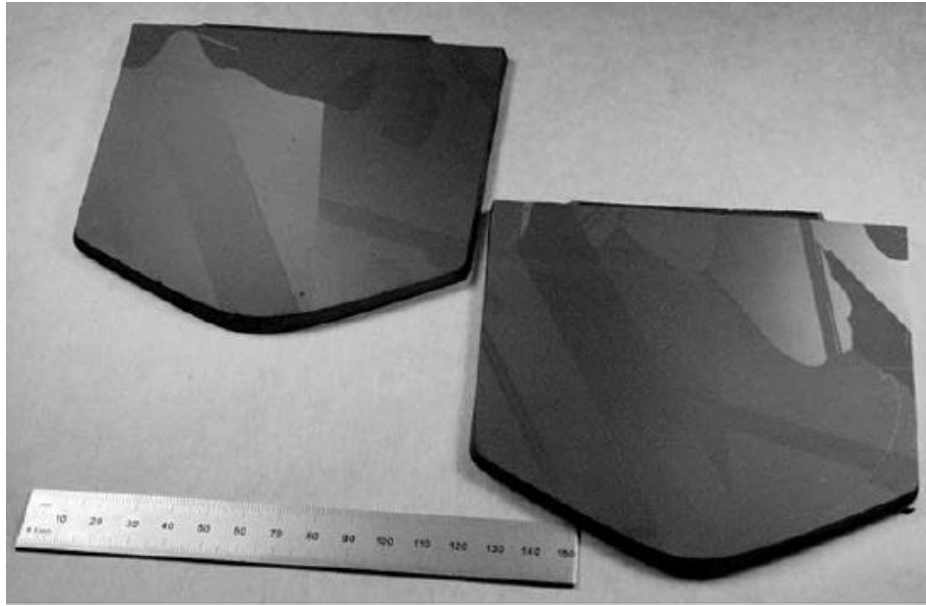
- Radial uniformity through the crystal (wafer)
- Low impurity & defect concentrations
- No grain boundaries or mechanical defects

In this poor quality crystal, the “last-to-freeze” region is at the top of the crystal

The material in this region is highly polycrystalline, and contains voids

It is useless for electronic devices

CZT crystal growth & yield

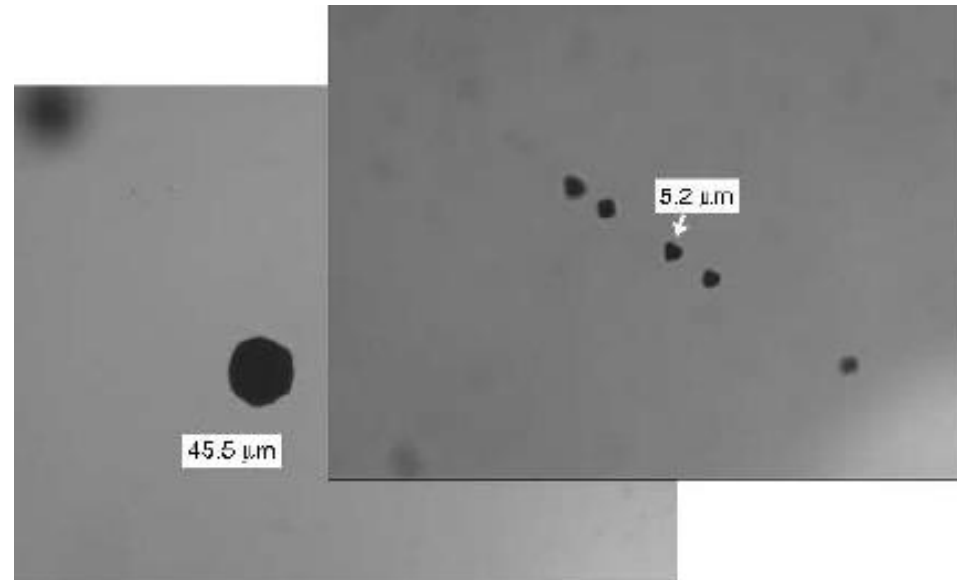


Early results in CZT crystal growth struggled to produce large-volume high quality material. Issues include:

- ❑ Impurities limit good charge transport
- ❑ Material is polycrystalline; the desired single-crystal regions must be cut from each wafer
- ❑ High defect concentration such as dislocations, “twins” and tellurium precipitates

IR microscopy used to assess Te inclusions, formed from Te-rich melt:

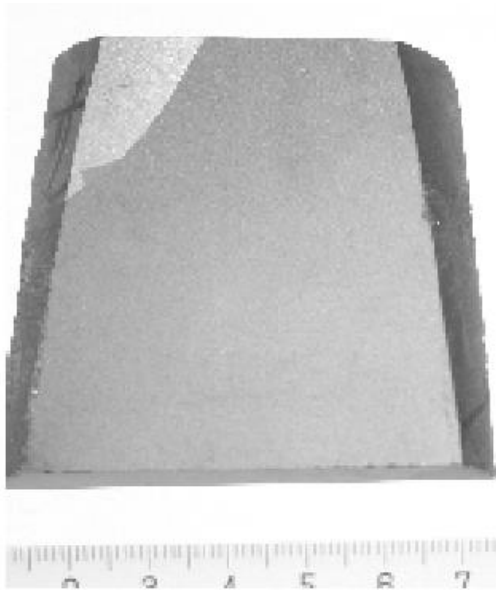
- ❑ Mainly triangular or polyhedron shape
- ❑ Often located along grain boundaries
- ❑ Te inclusions act as trapping sites, over a large range



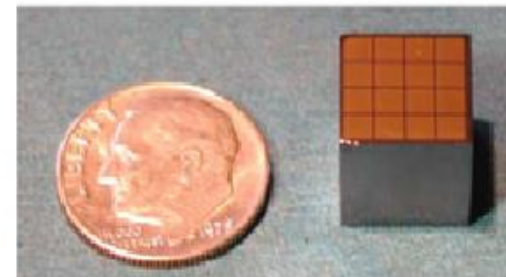
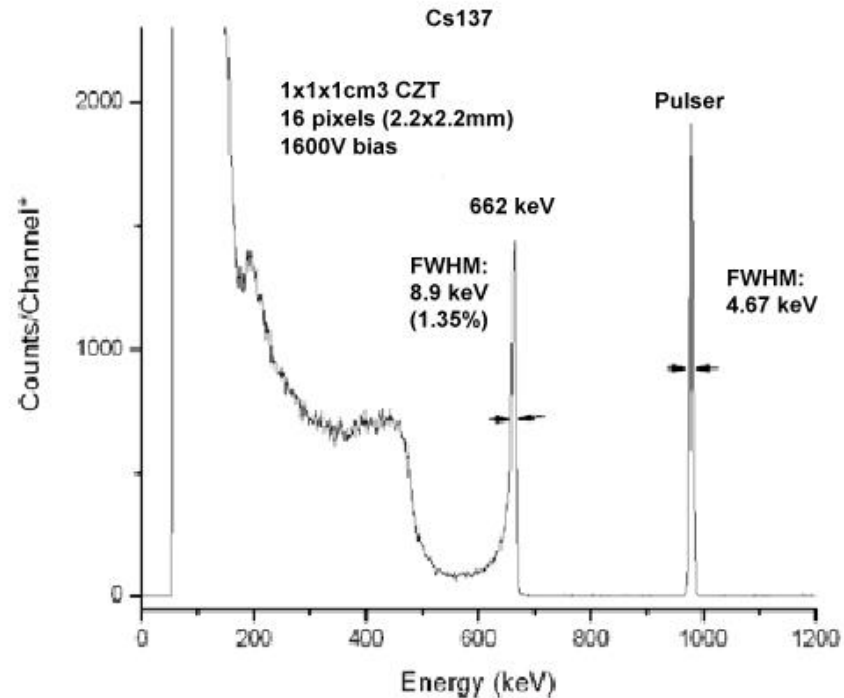
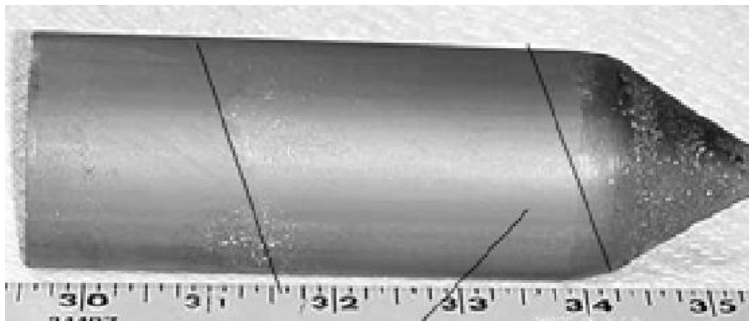
Pixel detectors fabricated from CZT

Some of the best quality CZT crystal is produced for use in pixellated gamma ray imaging detectors – uses include medical imaging and security detection

Excellent charge transport is now available, eg. resistivity $\rho=3 \times 10^{11} \Omega \text{cm}$, and $\mu\tau_e=1.8 \times 10^{-2} \text{ cm}^2/\text{V}$



4x4 pixelated devices
have shown very good
resolution
 \Rightarrow 1.35% FWHM at
662 keV



CZT pixel detectors for space imaging

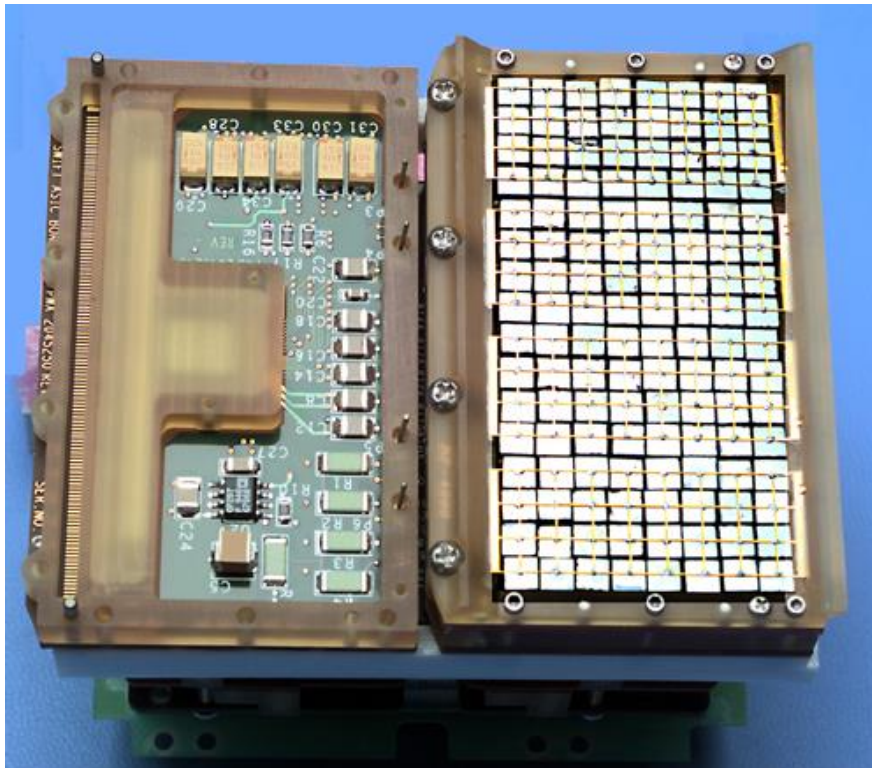
SWIFT CZT detector array:

❑ Contains 32768 elements of 4x4x2mm CZT, forming an array detector 1.2 x 0.6 m

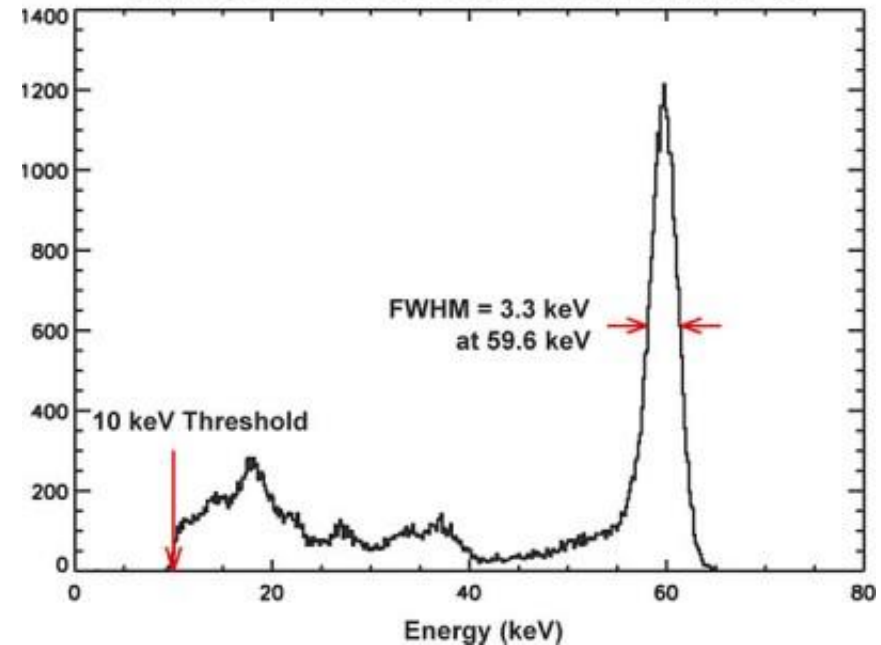
❑ The coded aperture mask is ~54,000 lead tiles

The INTEGRAL project used a similar CdTe detector array with 16384 CdTe pixels,

The typical performance of a single CZT module is 3.3 keV FWHM at 60 keV (5.5% FWHM):



241Am Spectrum for Module 001, Detector 15

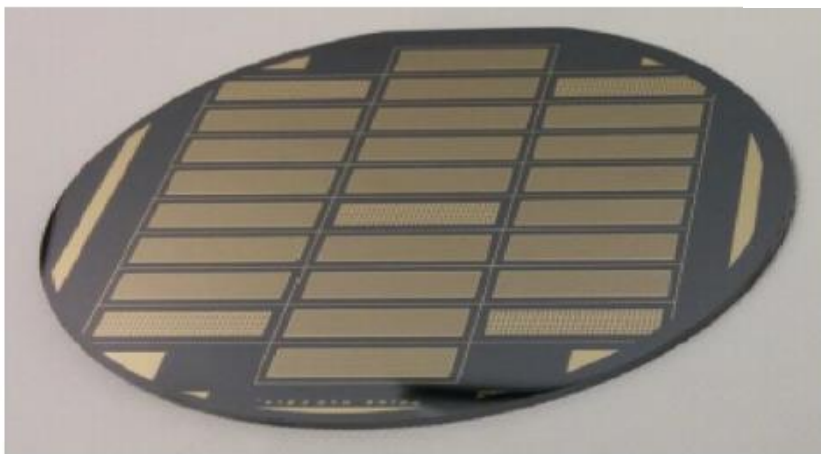
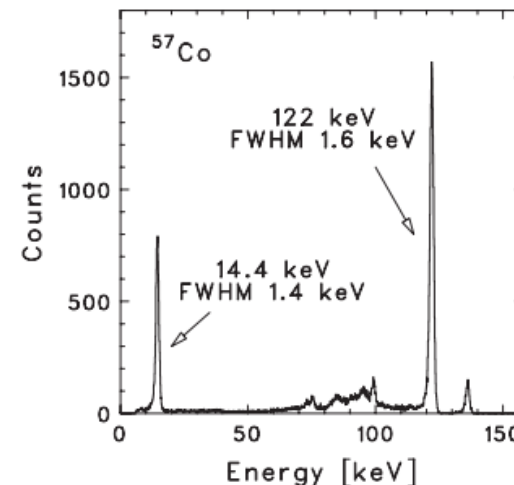
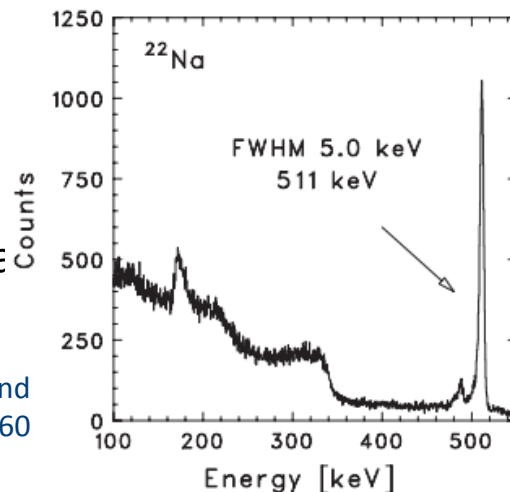


Current status of CdTe and CZT

Commercial availability of high quality CdTe and CZT remains with a small number of manufactures. The leading supplier of CdTe remains Acrorad (Japan) and the 2 dominant CZT suppliers are Redlen (Canada) and eV Products/Kromek (USA).

CdTe is normally used at only 0.5mm thickness to avoid field instability issues. Spectra show pixel energy resolution of 1.6 keV at 122 keV and 5.0 keV at 511 keV.

Acrorad 0.5mm thick CdTe pixel detector at T=-20 C and 1200 V. K. Oonuki et al, NIM A573 (2007) 57-60



CZT is now mainly commercially grown by the Travelling Heater Method (THM) which was pioneered by Redlen.

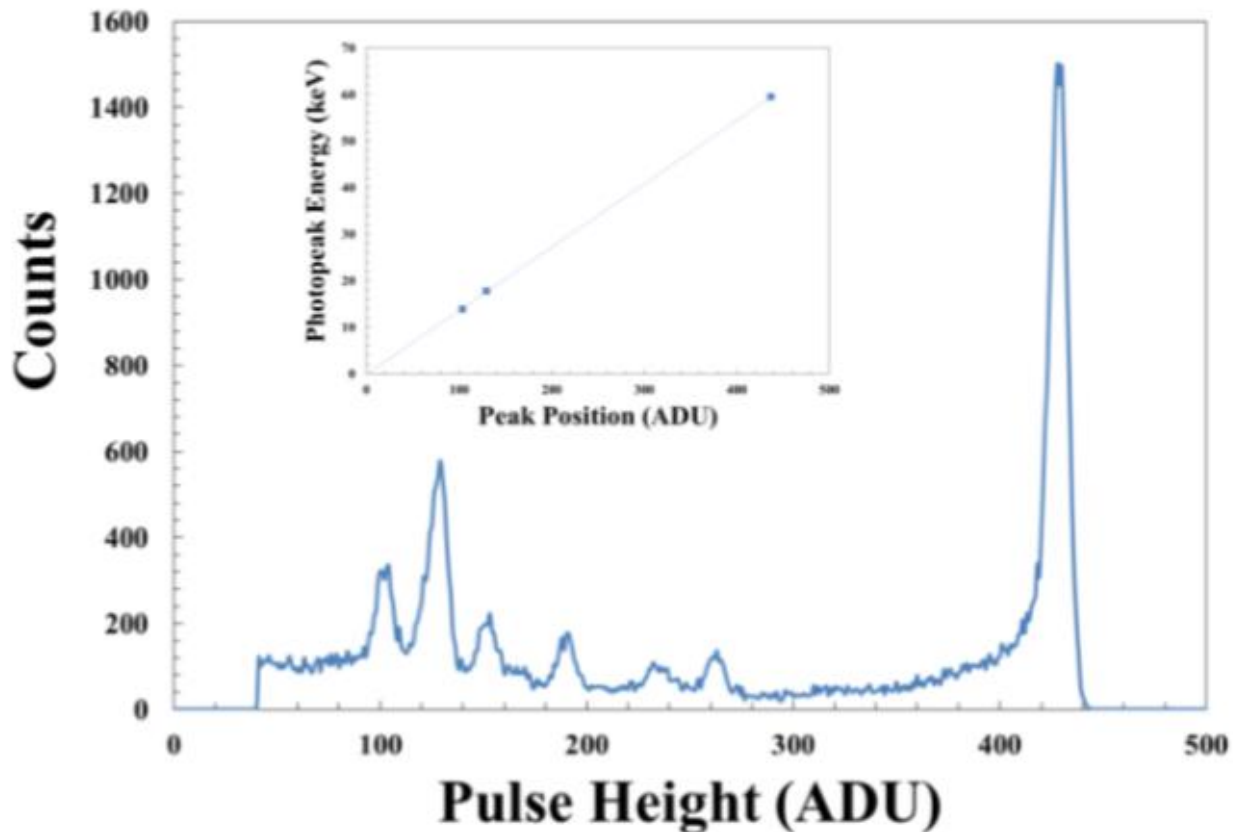
Whole wafer material is increasingly becoming available, compatible with conventional industrial processing.

3 inch diameter CZT wafer grown using THM growth and fabricated using wafer level processing (WLP).

CZT spectroscopy at low rates

Various groups have reported good photon resolution from thin CZT, typically optimised for energies below 150 keV

The HEXITEC collaboration have demonstrated spectroscopic pixel detectors on 2mm thick Redlen CZT with a 250 μ m pitch. The typical single pixel resolution is 1.8 keV FWHM:



Single pixel
spectrum at 300K,
1000V bias

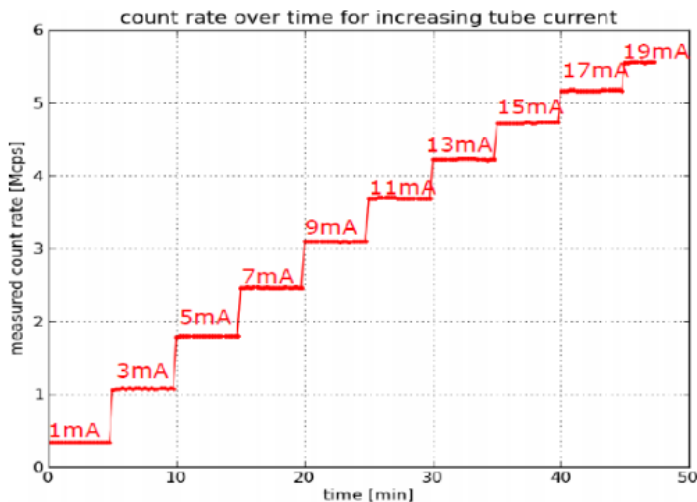
CZT performance at high flux

Redlen offer a variant of their THM grown CZT for use in high flux environments which has reduced impurity and defect concentrations

The objective is to minimise charge trapping and so reduce polarisation effects at high flux.

The main improvement has been in hole transport, with hole $\mu\tau$ improving from $\sim 10^{-5}$ to $\sim 10^{-4}$ cm^2/Vs . Stable performance is seen at count rates of 200 Mcps/ mm^2

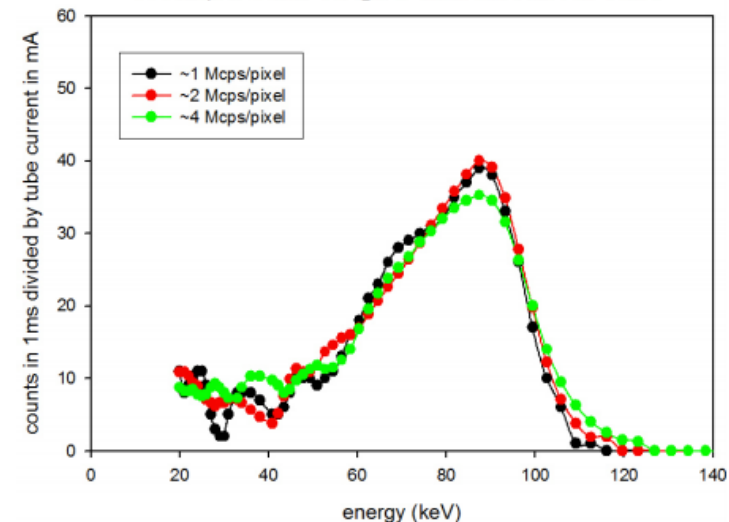
	$\mu_e\tau_e$ ($\times 10^{-4}$ cm^2V^{-1})	μ_e ($\text{cm}^2\text{V}^{-1}\text{s}^{-1}$)	τ_e ($\times 10^{-6}$ s)	$\mu_h\tau_h$ ($\times 10^{-4}$ cm^2V^{-1})	μ_h ($\text{cm}^2\text{V}^{-1}\text{s}^{-1}$)	τ_h ($\times 10^{-6}$ s)
High Flux CdZnTe	11 ± 6	940 ± 190	1.2 ± 0.8	2.9 ± 1.4	114 ± 22	2.5 ± 1.4
Standard CdZnTe	100	1100	11	0.2	88	0.2



Direct beam tests using a tungsten X-ray tube at 60kvp and 3mm Al filter

Photon counting pixel detector with 1mm pixel pitch, at up to 4 Mcps/pixel

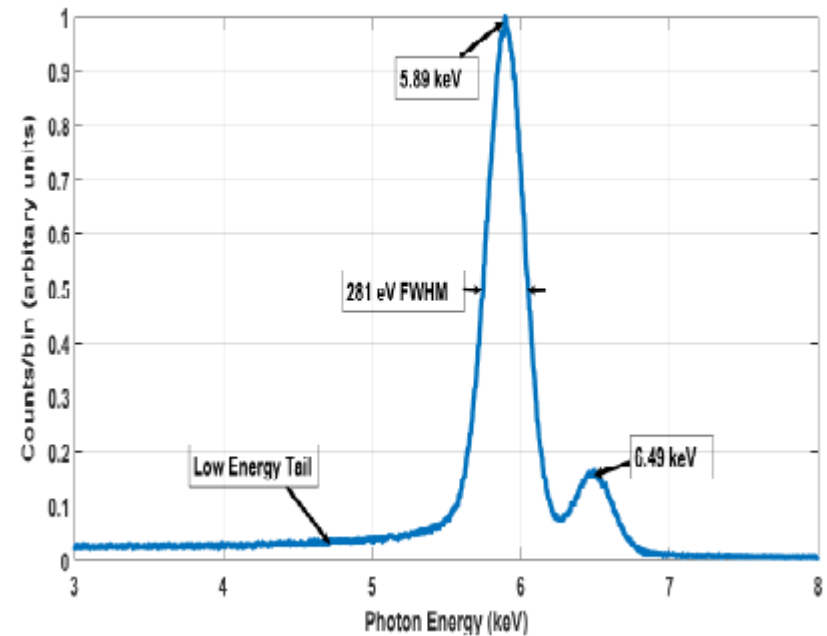
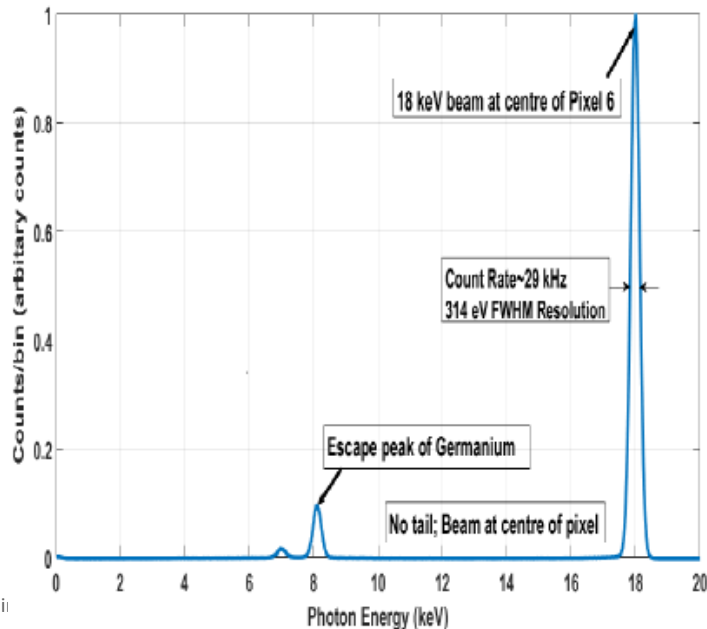
110 kVp & 1 mm Cu @ 20 cm from 1 mA to 4 mA



Germanium as the 'gold standard'

Germanium pixel detectors remain the 'gold standard' for high resolution imaging. Resolution near to the Fano limit is obtained by:

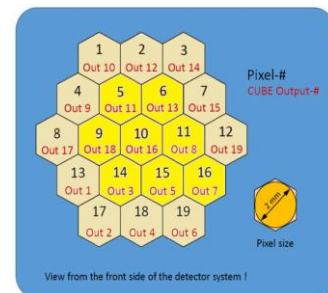
- Cryogenic cooling to suppress dark currents
- A small W value => creation of many electron/hole pairs per MeV
- Extremely high purity material with excellent energy resolution



^{55}Fe spectrum with a $6\mu\text{s}$ shaping time

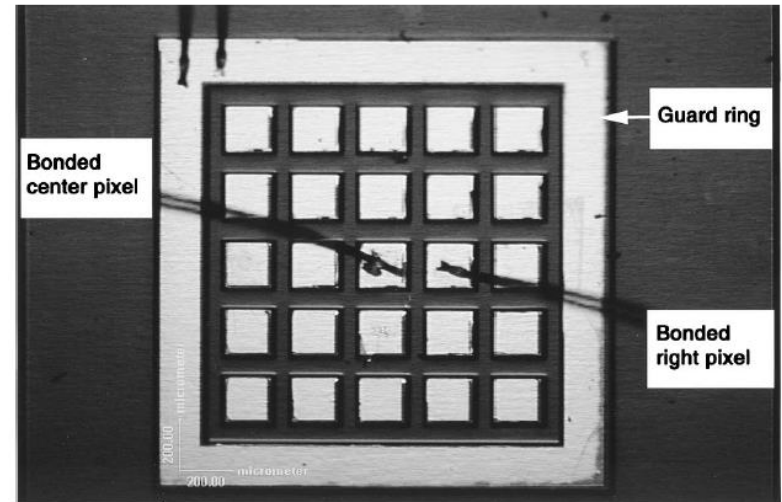
18 keV photons incident on a Ge pixel, showing the k_{α} and k_{β} escape peaks at $E_{PK}-9.8\text{ keV}$ and $E_{PK}-11.0\text{ keV}$

N. Tartoni et al, IEEE Trans Nucl Sci. 2017 in press.

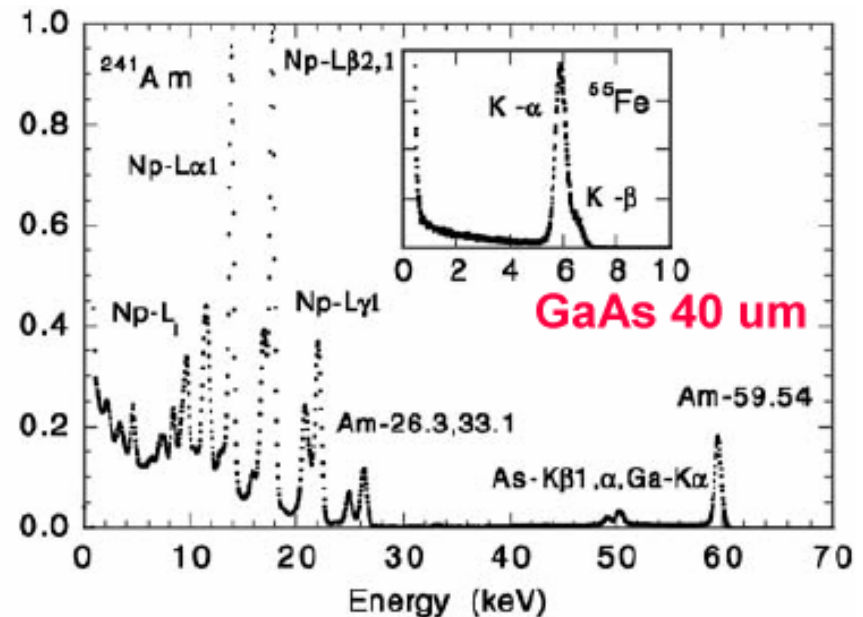
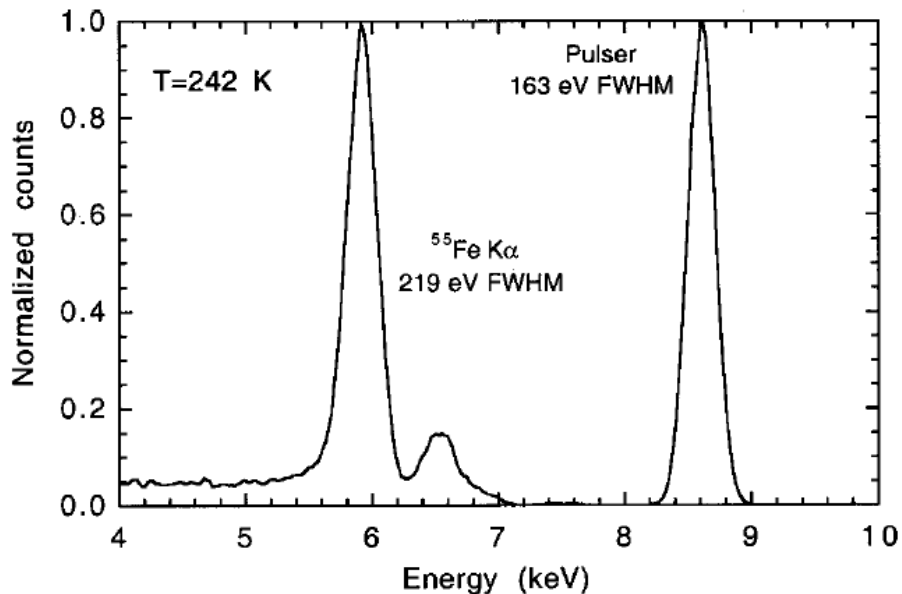


Early work on GaAs detectors

- High resolution performance was demonstrated in epitaxial GaAs, developed by ESTEC (ESA) in 2001
- Fano-limited performance was achieved, with full depletion of $\sim 40\mu\text{m}$ of GaAs
- This material had some availability through Metorex (Finland)



A. Owens et al, JAP 90 (2001) 5376

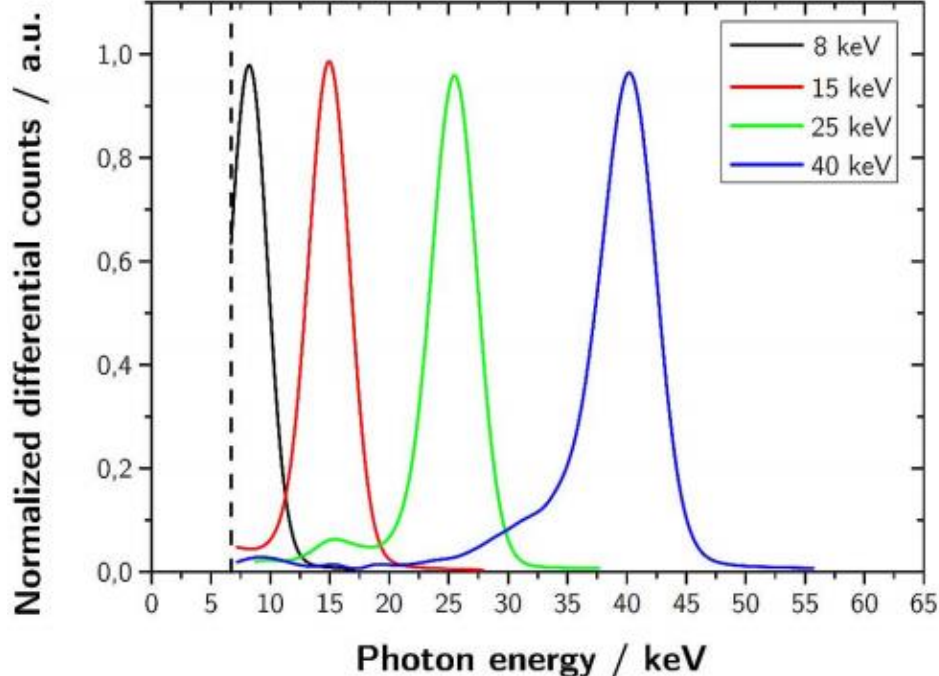


Recent results from GaAs

The conventional method of growing semi-insulating GaAs wafer is by Liquid Encapsulated Czochralski (LEC) growth. This materials has several problems:

- High leakage currents
- Short carrier lifetimes, due to deep level traps such as “EL2”
- Non-uniform electric field distributions.

Over the last 20 years the group at Tomsk have developed a chromium-compensated method to produce SI GaAs with good charge transport properties. The sensitive thickness of these wafers is $\sim 1\text{mm}$



Energy response function of 500 μm thick GaAs:Cr coupled to Medipix3 at 55 μm pixel pitch.

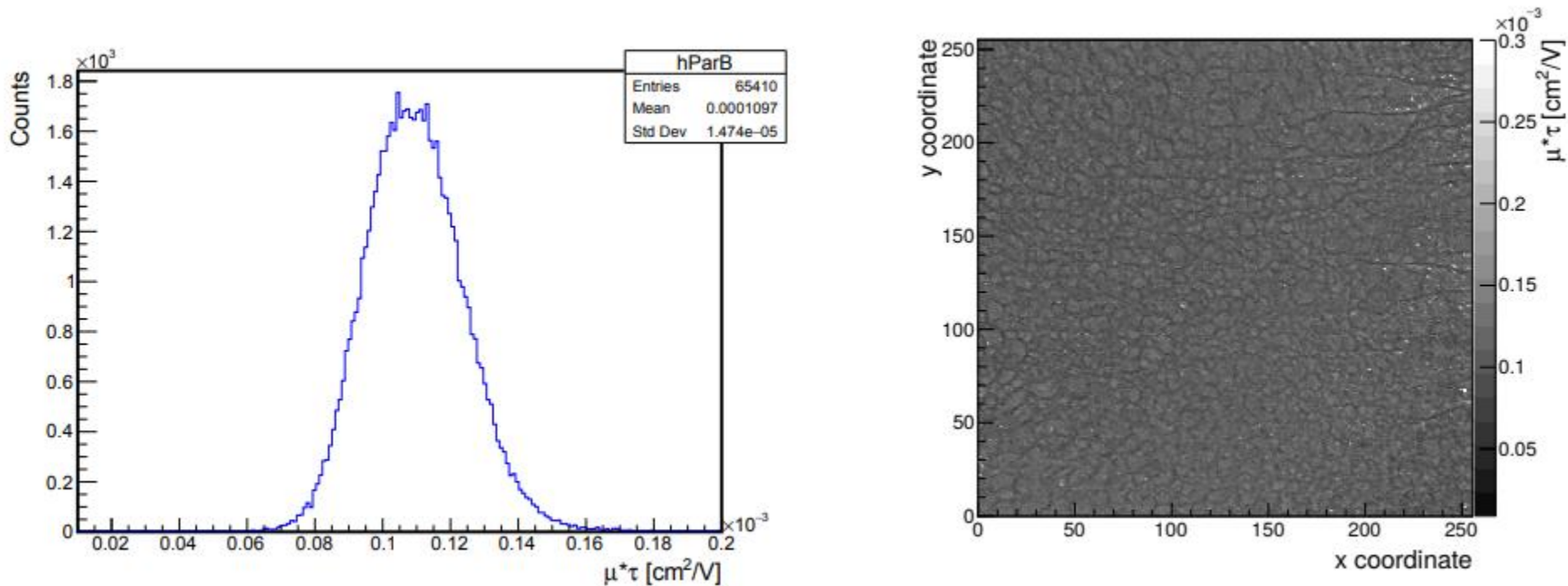
The escape peak at ~ 15 keV is just visible in the 25 keV data

G.I. Ayzenshtata , NIM A531 (2004) 121, E. Hamann et al, IEEE Trans Med Imag 34 (2015) 707-715

Charge transport properties of GaAs:Cr

GaAs:Cr was bonded to Timepix to assess the material performance. At 20C the material resistivity is $\sim 10^8 \Omega\text{cm}$ (equivalent to 0.05nA per pixel).

Electron $\mu\tau$ was measured using 15.7 keV photons from zirconium, with an average range of 25 μm from the cathode contact.

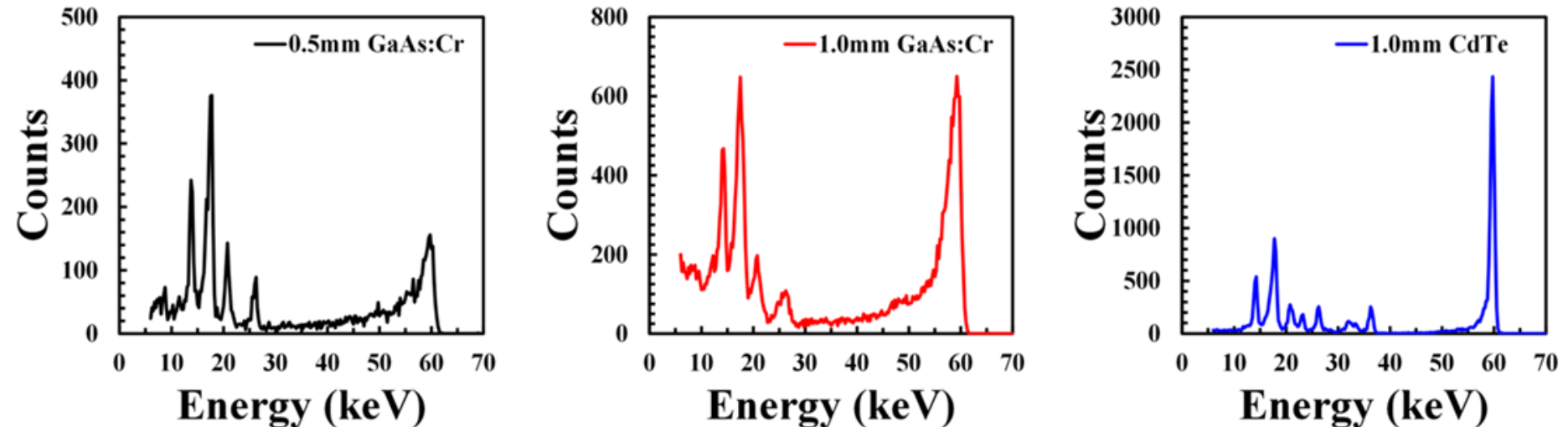


The electron $\mu\tau$ distribution from all pixels was well defined, with a mean $\mu\tau$ value of $1.1 \times 10^{-4} \text{ cm}^2/\text{V}$

Comparison of GaAs with other materials

The spectroscopic HEXITEC pixel detector has produced a direct comparison of the spectroscopic performance GaAs:Cr against CdTe

HEXITEC
HIGH ENERGY X-RAY IMAGING TECHNOLOGY



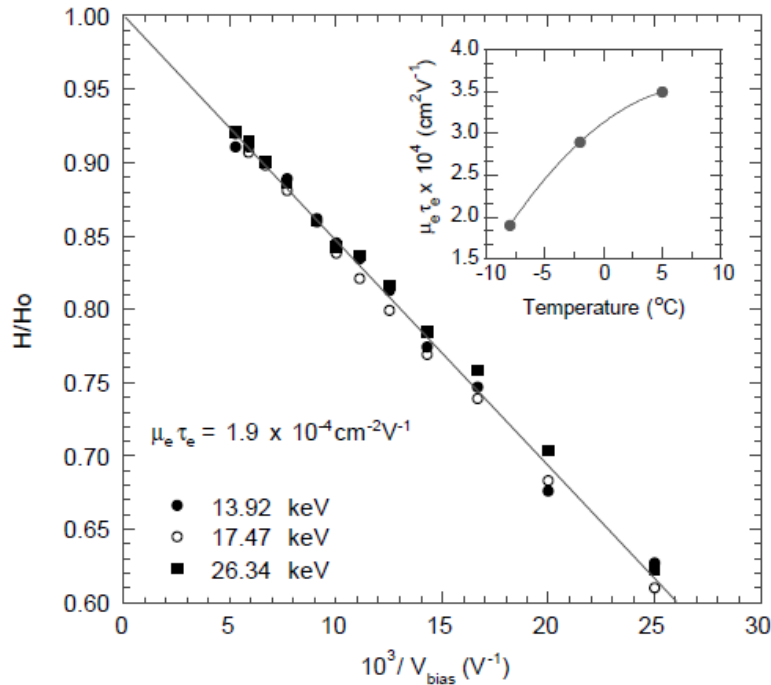
Room temperature ^{241}Am single pixel spectra from 250um pitch HEXITEC detectors after charge sharing discrimination.

The 0.5mm GaAs:Cr sensor performs very well at energies <30keV. It also has reduced escape peaks due to the lower energy of the Ga and As florescence X-rays.

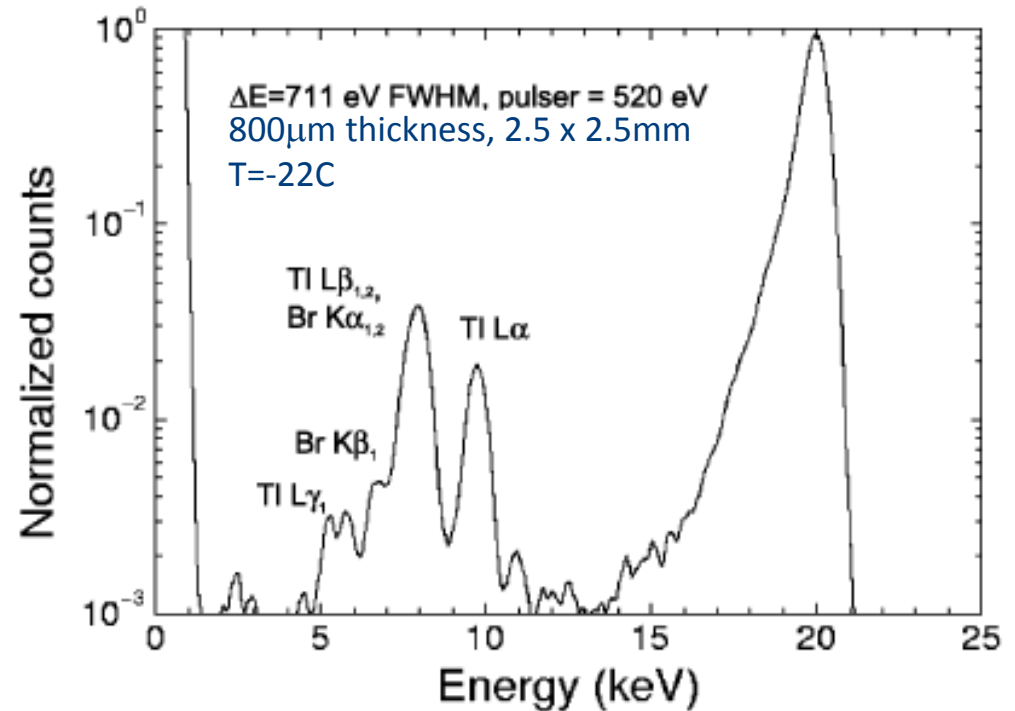
At higher energies depth of interaction effects have a negative effect on the spectroscopic performance due to the increased contribution of holes.

Early TlBr spectroscopy

TlBr is an interesting detector material at very high Z (81 and 35) and with high density
It's a specialist material with very limited current commercial availability



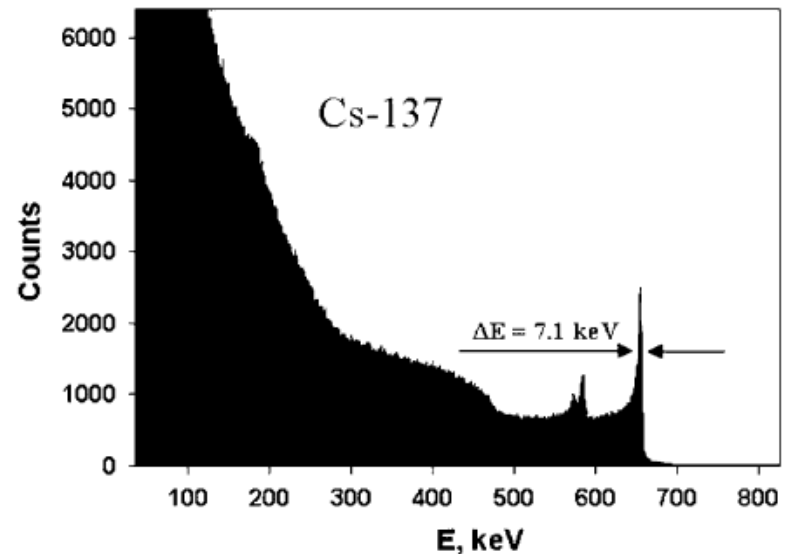
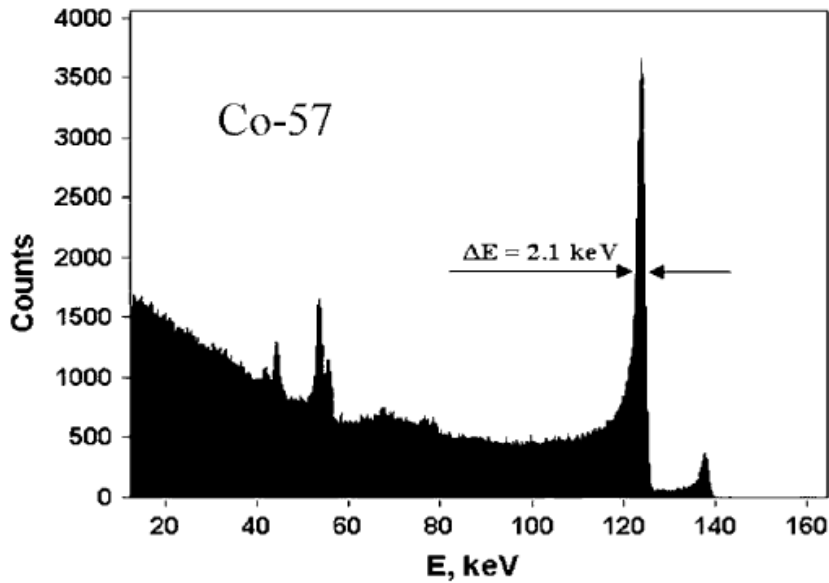
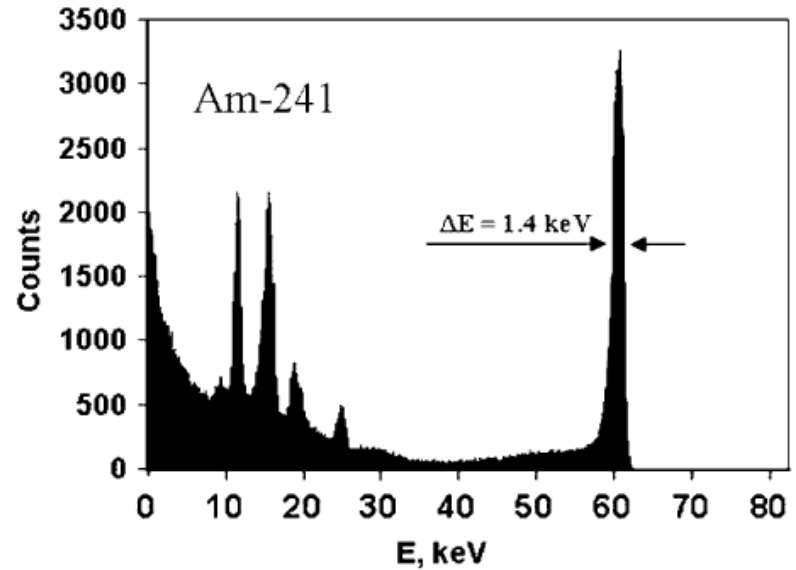
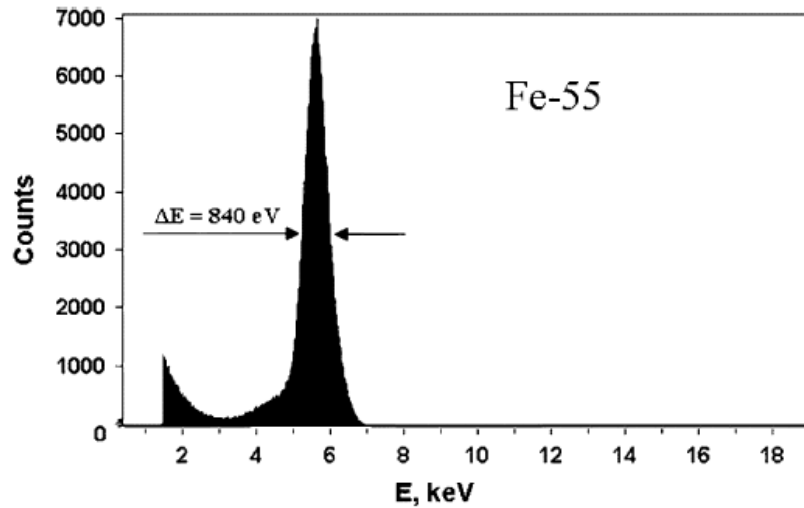
Cooling is necessary to ensure field stability.
Figure shows charge collection efficiency vs inverse bias voltage at -8C
Electron $\mu\tau = 1.9 \times 10^{-4} \text{ cm}^2 \text{ V}^{-1}$



Energy spectrum acquired from 20 keV photons
The escape peaks are from Br K_α , K_β and from Tl L_α , L_β and L_γ

Russian-grown TlBr material

TlBr ingots grown by Bridgeman-Stockbarger method. TlBr planar detector, thickness 2mm, at T=-40C



TlBr detectors from RMD

TlBr Spectroscopic Performance

Detector	Date	Overall Resolution	Best Pixel Resolution
58A3R	June 2010	1.32%	0.93%
58A4L	May 2010	1.98%	1.04%
48A2R	March 2011	4.26%	3.16%
935-16B1R	May 2011	0.97%	0.73%
935-16B1L	June 2011	1.45%	1.07%
44B2L	September 2011	2.64%	1.81%
70BA1L	December 2011	1.76%	1.22%
70BA1R	December 2011	1.19%	1.05%
47AR	April 2012	1.89%	1.09%
44A12R	June 2012	4.28%	2.94%
43A4R	September 2012	3.87%	2.89%
70BA2R	September 2012	2.98%	2.04%
44AB1R	September 2012	1.82%	1.37%

5mm thick pixel detectors operated at -20C to minimise field polarisation.

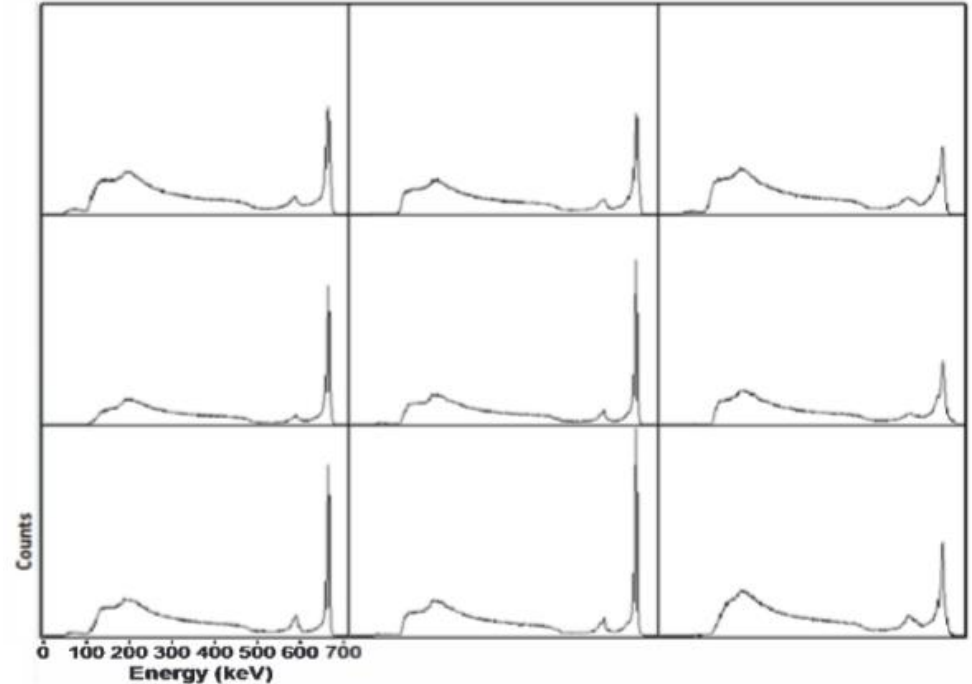
Depth-corrected, pixel-by-pixel energy spectra for detector

The energy resolution in the best pixel is 0.77% FWHM at 662 keV

More recently TlBr has been extensively developed by RMD

Results from TlBr pixel detectors have been reported, eg. 3x3 pixel arrays on a 5mm pixel pitch.

High bias voltage of 1000V is used to maximise electron transport



Other Materials: High-Z polycrystalline

Polycrystalline thick film high-Z ($Z \geq 80$) materials have been extensively studied for X-ray imaging applications. Their main potential is for large areas.

Material	Z	density	mobility	E_G	resistivity
<u>Iodides:</u>		g/cm^3	cm^2/Vs	eV	Ωcm
Hgl₂	80/53	6.4	50	2.1	10^{13}
Pbl₂	82/53	6.2	53	2.5	10^{12}
Bil₃	83/53	5.8	48	1.7	10^{12}
<u>Bromides:</u>					
TlBr	81/35	7.6	75	2.7	10^{12}
PbBr	82/35	-	-	2.5-3.1	-
<u>Oxides:</u>					
PbO	82/8	9.5	-	1.9	-

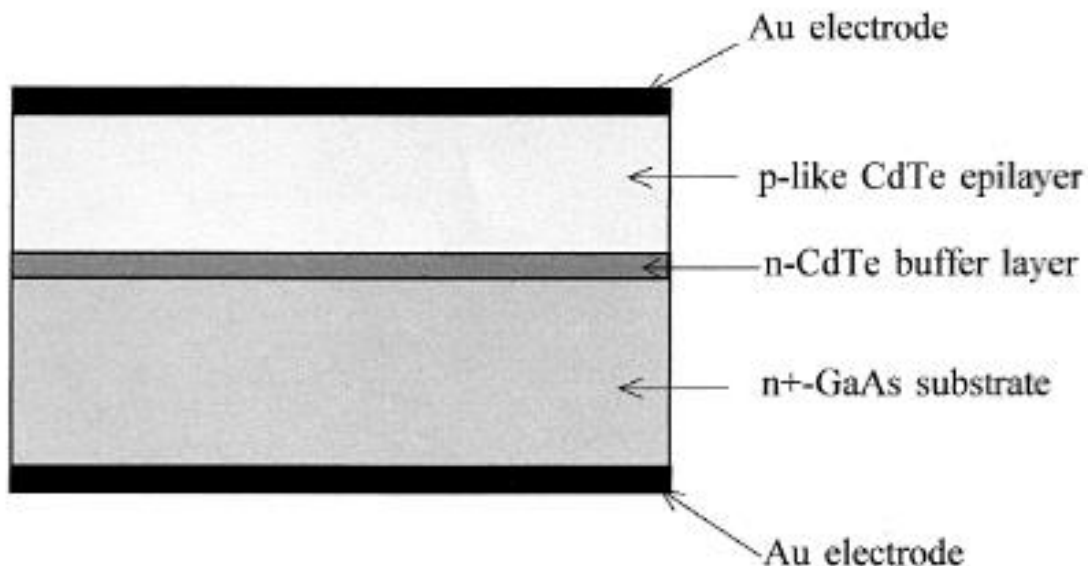
The iodide and bromide families have many suitable candidates:

- Detailed studies of Hgl₂ and Pbl₂ have been carried out
- Hgl₂ shows superior dark current and charge transport properties
- Promising results from polycrystalline TlBr

Large-area epitaxial CdTe grown by MOVPE

Metal-organic vapor-phase epitaxy (MOVPE) is capable of growing large-area epitaxial thick films, eg. up to 200 μm thick

- MOVPE growth of CdTe or CZT on GaAs or Si substrates, produces uniform mono-crystals
- GaAs substrates provide a good lattice match and strong adhesion



❑ Iodine-doped buffer layer grown onto substrate (10^{17} cm^{-3})

Prevents Ga diffusion into epitaxial CdTe layer

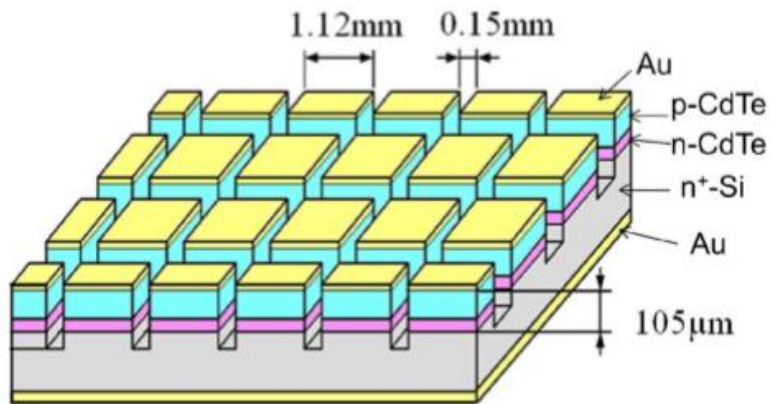
❑ undoped p-type epitaxial CdTe layer grown at 415-560 $^{\circ}\text{C}$

❑ rectifying p-n junction formed at the CdTe/GaAs interface

Epitaxial CdTe pixel sensor

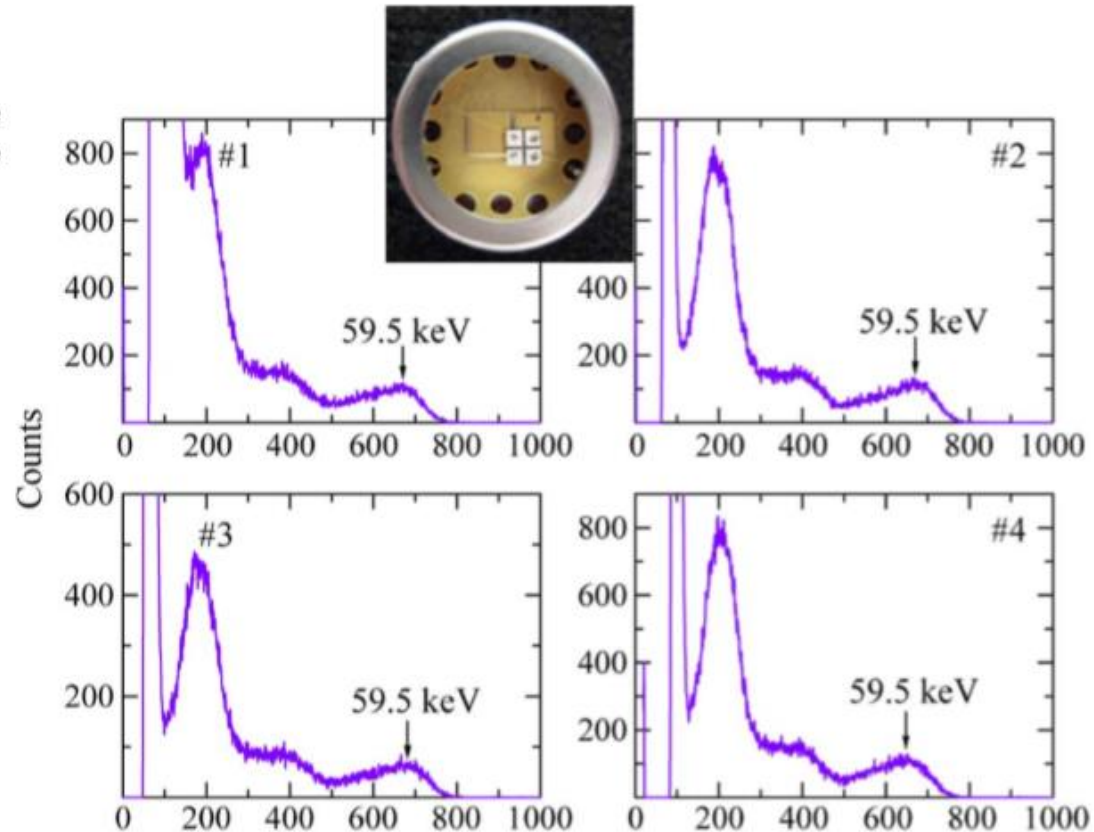
First prototypes have been reported for large area MOVPE CdTe pixel detectors

8 x 8 pixel array on 1.27mm pixel pitch, with mechanical grooves to define each pixel. The CdTe sensor layer is 100 - 260 μm thick.



Leakage current are high for this device, $\sim 150 \text{nA/cm}^2$ at 150V bias.

Modest spectral performance with a broad 59 keV photopeak at room temperature



Conclusion

Detector materials are one essential part of our “fishing kit” for synchrotron detectors

In materials development that is always a compromise between performance, cost, and timescale.

Driven by the medical imaging market, CZT material has now started to deliver real detectors with “good enough” energy resolution

Operation of CZT at high rates continues to be a challenge, which must be solved by the medical and security markets.

Other high-Z materials are now providing niche solutions, eg: germanium, GaAs, and perhaps vapour phase materials